International Journal of Biological Macromolecules 343 (2026) 150226

Contents lists available at ScienceDirect

International Journal of Biological Macromolecules

journal homepage: www.elsevier.com/locate/ijbiomac

Immobilization of lignin nano/microparticles on plasma-modified polymer nanofibers

Lucie Janů [a], Nada Souawda [a], Resmi Anand [b], David Duday [b], Jiřina Medalová [c], Delphine Collard [b], David Nečas [a], Kateřina Polášková [a], Petr Ryšánek [d], Jean-Sébastien Thomann [b], Martina Janůšová [a], Lenka Zajíčková [a,e,*]

[a] Plasma Technologies, CEITEC, Brno University of Technology, Purkyňova 123, Brno, 612 00, Czech Republic
[b] Luxembourg Institute of Science and Technology (LIST), Maison de l'innovation 5, Esch-sur-Alzette, L-4362, Luxembourg
[c] Department of Experimental Biology, Faculty of Science, Masaryk University, Kamenice 753/5, Brno, 62500, Czech Republic
[d] Centre for Nanomaterials and Biotechnology, Faculty of Science, University of J. E. Purkyne in Usti nad Labem, Pasteurova 3632/15, Ústínad Labem, 40096, Czech Republic
[e] Department Condensed Matter Physics, Faculty of Science, Masaryk University, Kotlářská 2, Brno, 61137, Czech Republic

ARTICLE INFO

Keywords:
Plasma processing
Immobilization
Lignin

ABSTRACT

Lignin, one of the most abundant renewable phenolic biopolymers, exhibits antibacterial, antioxidant, and UV-blocking properties. Synthesizing lignin nanoparticles (NPs) opens up new applications by offering advantages over bulk lignin, providing a high specific surface area, increased reactivity, and water solubility. We discovered that lignin sizes and concentrations sufficient to elicit an antimicrobial effect in suspension against *E. coli* were simultaneously cytotoxic *in vitro*, underscoring the need for careful dose optimization in biomedical applications. Since polymer nanofibers (NFs) serve as excellent carriers for NPs, we aimed to immobilize four types of lignin nano/microparticles (15 nm–2 μm in diameter) onto polymer nanofibrous mats. Dip-coating of lignin particles from a water colloid/suspension onto the NF mats proved to be the most reproducible and homogeneous method. To address the issues related to the hydrophobicity of synthetic polymers and to mediate particle attachment, we explored plasma-based surface modifications of NFs, namely O_2 plasma treatment and deposition of carboxyl and amine plasma polymers (PPs). Besides particle immobilization, plasma modification improves the biocompatibility and bioactivity of NFs. Overall, up to 15% of lignin initial mass was bound to NFs, resulting in a high surface coverage (~50%). Among the tested modifications, positively charged amine PP coatings demonstrated the highest efficiency and versatility, yielding stable attachment of negatively charged lignin nano/microparticles even during immersion into water. Since the water contact angle of pristine and carboxyl-PP-coated NFs was similar, 119–121°, we proposed that these mats immobilize lignin particles through hydrophobic interactions, resulting in partial particle release upon immersion in water.

1. Introduction

Lignin is the second most abundant renewable aromatic biopolymer with versatile chemistry and substantial valorization capability. Considering its structure, which features phenolic units [1], lignin holds immense potential for various applications. However, its heterogeneous chemical structure, which highly depends on the biomass source and the extraction and purification methods, is partly responsible for the under-utilization of lignin, with only 5% of the more than 50 million tons produced annually being converted into functional materials [2]. Proceeding from the role of lignin in providing plant structural integrity and protection against pathogens [3], lignin cannot only improve the mechanical properties of polymeric materials but also contribute to antibacterial, antioxidant, and UV protection functionalities [1]. The antibacterial activity of lignin relies on a nonspecific mode of action associated with the presence of hydroxyl and carboxylic groups [4]. Additionally, phenolic functionalities in lignin provide it with antioxidant activity through free-radical scavenging [5]. Therefore, lignin also stands out as a promising antioxidant agent in various applications, including food processing and pharmaceutical products, offering a safer alternative to cytotoxic synthetic antioxidants [6].

Technologies allowing lignin synthesis in nano/microparticle form have emerged as a potential valorization pathway, offering advantages over the bulk material in a high specific surface area, increasing lignin

* Corresponding author at: Department Condensed Matter Physics, Faculty of Science, Masaryk University, Kotlářská 2, Brno, 61137, Czech Republic.
E-mail address: lenkaz@physics.muni.cz (L. Zajíčková).

https://doi.org/10.1016/j.ijbiomac.2026.150226
Received 29 September 2025; Received in revised form 20 December 2025; Accepted 11 January 2026
Available online 17 January 2026

reactivity, and overcoming the poor water solubility [7]. Additionally, controlling morphology by fine-tuning the shape and size of particles [8] enables the adjustment of the stability and cytotoxicity of the colloidal dispersion. However, a carrier matrix is essential to realize the new potential that lignin nanoparticles (NPs) can offer. In this regard, electrospun synthetic polymeric nanofibers (NFs) with their high porosity, 3D architecture, and interconnected pore network have appeared as a prospective solution [9]. The most common approach to combine NPs with NFs is a direct incorporation by adding the NPs to a polymer solution before electrospinning. Integration of lignin NPs improved the mechanical properties of NFs in terms of tensile strength, enhanced thermal stability, and UV resistance [10]. Focusing on bioapplications, composite NFs with embedded lignin NPs exhibited increased wettability, promoting proper cell growth in nerve regeneration [11] or pre-osteoblastic cell line proliferation, attachment and osteogenic differentiation for bone tissue engineering [2]. The NF/NP nanocomposite also showed boosted biodegradability, along with excellent antioxidant and antibacterial efficacy [2].

If the lignin should be accessible for the given application, the immobilization of lignin NPs on the surface of pre-prepared NFs can be a better strategy than adding NPs to the electrospinning solution. This surface-functionalization approach can also simplify the preparation of polymer nanofibrous mats, as adding any material to a polymer solution for electrospinning will alter the optimum electrospinning conditions. A straightforward method involves dip-coating NFs in an NP suspension, as demonstrated for TiO_2 NPs [12,13]. However, since synthetic polymers suffer from low surface energy and inertness, more elaborate methods enriching NF surface with functional polar groups have been studied, including the co/electrospinning with polymers bearing amino groups [14–19] or grafting of NFs with amine-containing compounds using wet chemistry [20,21]. The introduced amino functionalities subsequently facilitate hydrogen bonding [15,18], electrostatic interaction [16,17,19–21], or covalent attachment [14] of appropriately functionalized metallic NPs (Au, Ag, Pt, or ZnO), typically via dip-coating from suspension. Although co-electrospinning is promising, it faces challenging optimization accompanied by possible immiscibility of polymers and the use of hazardous solvents [22]. Similarly, wet chemistry encounters difficulties related to lengthy multi-step processes and the excessive use of solvents [23].

Plasma-based surface modifications allow for low process temperatures and are solvent-free. Therefore, they proved to be an effective and environmentally friendly surface-independent processing strategy for polymers that introduces surface functional groups required for the stable immobilization of other compounds or materials. A few-monolayer-thick surface region of a bulk material can be modified by plasma treatment. Since polymer chains tend to rearrange, diminishing the treatment effect, thicker surface modification provided by plasma-enhanced chemical vapor deposition (PECVD) of plasma polymer (PP) thin films is often preferred for introducing chemical functional groups to the material surface without altering the bulk characteristics. Different PPs have already been successfully employed to bind diverse NPs to the substrate. Suitably functionalized metallic Au or Ag NPs were electrostatically immobilized to amine [24–26], methyl [27,28] and aldehyde-terminated [29] PPs or covalently bonded to oxazoline PPs [30–33], as has been extensively studied by Vasilev's group. Several other researchers utilize amine PPs to bind again metallic [34–36] or hybrid polymer-metallic NPs [37,38]. However, the research has so far focused almost exclusively on immobilizing metallic NPs on PP-coated flat non-structured substrates with a few exceptions. Joseph et al. [39] immobilized Au NPs on 3D-printed PCL macroporous scaffolds modified by amine PPs and Aksit et al. [40] plasma polymerized acrylic acid on various nonwoven fabrics to bind Ag-doped TiO_2 NPs. Nevertheless, since features of these substrates (sizes of pores, fibers, etc.) are in the macroscale, orders of magnitude larger compared to NFs, deposition and immobilization outcomes are not automatically translatable when coating NF mats, as we discussed in Michlíček et al. [41].

In this work, we utilize low-pressure PECVD, which remains underexplored for the immobilization of NPs onto NFs, in contrast to well-established wet-chemistry-based methods. PECVD of thin films on polymer NFs is relatively rare, with only limited literature addressing this possibility [42–44]. However, we have already showed that temperature-sensitive PCL NFs can be coated without compromising their structure with amine [45] or carboxyl [46] PPs. Building on our former findings, we demonstrated for the first time that plasma polymers with amino groups can be used for stable immobilization of lignin nanoparticles. Besides mediating the attachment of NPs, we have reported previously that PP-coated PCL NFs significantly promote cell adhesion and enhance cell proliferation compared to pristine NFs [46–48]. Moreover, the present study systematically investigates the effects of three different plasma surface modifications, namely oxygen treatment, amine and carboxyl PP depositions, on the immobilization of four types of non-metallic lignin nano- and microparticles onto PCL NFs. Thus, it establishes low-pressure PECVD as a promising strategy for functionalizing polymer NFs, offering a versatile platform for NP immobilization and enhanced bioactivity. Furthermore, we focused on determining lignin particle concentrations *in vitro*, which are already antimicrobial but do not impose cytotoxic effects on cells, an often-overlooked point.

2. Methodology

2.1. Lignin nano/microparticles

2.1.1. Synthesis

Four types of lignin particles, labeled 15NPs, 50NPs, 300NPs and MPs, were synthesized at the Luxembourg Institute of Science and Technology (LIST). 15NPs and 50NPs particles were prepared by the solvent-shifting method (Fig. S1), as reported by Manisekaran et al. [49], from kraft lignin powder (BioPiva™ 190) received from UPM Biochemicals, Finland. Its elemental composition is: 62.5 at.% of carbon, 6.1 at.% of hydrogen, 2.0 at.% of sulphur, and <0.1 at.% of nitrogen [49]. The kraft lignin was dissolved in either dimethylsulfoxide for 15NPs particles (DMSO, 99.9%, anhydrous, Sigma-Aldrich, Belgium) or tetrahydrofuran for 50NPs particles (THF, ≥99.9%, anhydrous, Sigma-Aldrich, Belgium) to achieve a concentration of 20 mg/ml. THF or DMSO served as the solvents and deionized water as the nonsolvent. The 50 ml of kraft lignin solution was immediately injected into 1 l of deionized water while stirring at room temperature. The mixture was stirred continuously for 20 min to complete the lignin particle formation successfully. The solvent was removed either by rotary evaporation (THF) or dialysis (DMSO) using a dialysis membrane (MWCO 12–14 kDa, Spectra/Por®) at room temperature under slow stirring for three days. It resulted in a colloid of particles in water. To obtain the dried powder, the colloids were concentrated in a rotavap to reach a concentration of 30 mg/ml and freeze-dried for several days. 300NPs particles were also synthesized by the solvent-shifting method; 50 ml of kraft lignin solution (5 mg/ml) in THF (solvent) was added to 100 ml of 1% acetic acid (nonsolvent, pH~3). THF was removed by rotary evaporation and acetic acid by dialysis in Milli-Q water for 3 days using a dialysis membrane (MWCO 12–14 kDa, Spectra/Por®). MPs particles were prepared by spray drying a 50NPs colloid (1 mg/ml in Milli-Q water) using Buchi Mini Spray dryer B-290. Detailed physical characteristics of lignin particles can be found in Table 1.

2.1.2. Antimicrobial activity

Antimicrobial testing of lignin particles was accomplished at the Department of Experimental Biology of Masaryk University and at LIST. At Masaryk University, antimicrobial effects of lignin particles were tested on gram-negative *Escherichia coli* (*E. coli*). The methodology followed a modified version of the M26-A document of CLSI (CLSI, Methods for Determining Bactericidal Activity of Antimicrobial Agents) [50]. 100 µl

Table 1
Physical properties and chemical composition of lignin particles.

Label	Diameter (mm)[a]	Hydrodynamic size (N m)	PDI	Zeta potential (mv)	XPS		
					O (at.%)	C (at.%)	S (at.%)
15NPs	15	17 ± 8	0.15	−35 ± 5	23.6 ± 0.2	75.8 ± 0.2	0.6 ± 0.1
50NPs	50	90–100	0.15	−39 ± 5	22.6 ± 0.4	76.7 ± 0.4	0.67 ± 0.04
300NPs	320	300	0.10	−33 ± 5	24.8 ± 0.1	74.4 ± 0.1	0.8 ± 0.1
MPs	1200–2200	>1000	–[b]	−40 ± 7	22.0 ± 0.3	77.4 ± 0.2	0.61 ± 0.03

[a] Average diameter determined by SEM.
[b] Above the detection limit.

of *E. coli* (2.7×10^5 CFU/ml; CFU — colony-forming unit) in double-concentrated Lysogeny Broth medium was mixed with 100 µl of lignin colloid/suspension (particle concentration in medium = 0.4 mg/ml or higher) and cultivated for 24 h in Eppendorf™ tubes on a shaker (37 °C). The number of bacteria was assessed using the dilution method.

LIST carried out antimicrobial testing comparing the effect of MPs particles on gram-negative *E. coli* and gram-positive *Staphylococcus aureus* (*S. aureus*). MPs particles were tested using the microbroth dilution method under dynamic conditions. Briefly, the suspension of particles (20 mg/ml) was serially diluted in a growth medium, Mueller-Hinton Broth (MHB). One volume of the diluted suspension (50 µl) was added to an equal volume of bacterial inoculum (50 µl) in sterile 96-well polypropylene microtiter plates, giving a final bacterial concentration of 1×10^5 CFU/ml in each well. For each tested microorganism, sterility control wells (100 µl of sterile MHB) and growth control wells (50 µl of sterile MHB + 50 µl of bacterial inoculum) were prepared in the sterile 96-well microtiter plate. The inoculated 96-well polypropylene microplates were incubated at 37 °C for 16–20 h under agitation (180 rpm) and in a humidity chamber (RH > 90%). After a 24-hour incubation period, the dilution series was observed for microbial growth. 50 µl of the liquid medium was taken directly from each well and serially diluted in phosphate-buffered saline.

The bacterial concentration was determined using the plate count method. The most common estimation of antibacterial activity is a determination of minimum inhibitory concentration (MIC), which corresponds to the lowest concentration of antimicrobial agent needed to kill 99.9% of bacteria after incubation for 24 h under a standardized set of conditions [50]. The antibacterial activity was calculated as antimicrobial log reduction (ALR) by the equation

$$\mathrm{ALR} = \log_{10} \frac{N}{M} \tag{1}$$

where N and M are bacteria CFUs in the control and tested samples, respectively. The ALR must be ≥3 to consider the tested agent to be antimicrobial.

2.1.3. Cytotoxicity

The effect of lignin on cell viability was evaluated by ATP assay after its addition to culture media. Determining the relative amount of ATP in cell lysate (proportional to the number of living cells) was based on measuring chemiluminescence emitted by luciferase cleaving luciferin as long as ATP is present. 30 000 of cells, human fibroblasts (LF, spontaneously immortalized primary cell line) and keratinocytes (HaCaT, CLS Cell Lines Service GmbH/Cytion, Eppelheim, Germany) were seeded in 96-well plates in the volume of 90 µl of Dulbecco's modified Eagle's medium (DMEM, high glucose, Gibco, Thermo Fisher Scientific) with the addition of 10% fetal bovine serum (Gibco, Thermo Fisher Scientific), 1.2 mM L-glutamine (Gibco, ThermoFisher Scientific) and 100 U/ml Penicillin/Streptomycin (HyClone, Thermo Fisher Scientific). 10 µl of lignin colloid or suspension with a particular concentration was added. Cells were incubated for 2 days in the incubator (Thermo Fisher Scientific) at 37 °C in an air atmosphere with 5% CO_2 and 95% humidity. Afterwards, cells were washed with 100 µl of phosphate-buffered saline, 50 µl of the somatic cell ATP release reagent (Merck, Darmstadt, Germany) was added to each well, and cells were incubated at room temperature on a shaker for 10 min. 20 µl of lysate was mixed in a 1:1 ratio with a solution containing luciferase and luciferin mixture (BioThema, Handen, Sweden). In the shortest possible time, chemiluminescence was measured on a Hidex Sense plate reader (Hidex Oy, Turku, Finland). For each concentration and lignin type, at least 6 measurements were conducted. The relative value to control was calculated independently for each using a first-order bias-corrected ratio estimator.

2.2. Preparation of nanofibrous mats

2.2.1. Electrospinning of PCL nanofibrous mats

Polycaprolactone (PCL) nanofibrous mats were prepared by electrospinning from the PCL solution. PCL pellets (Mn 80 000, Merck, Darmstadt, Germany) were dissolved in a mixture of acetic acid (99%, Merck, Darmstadt, Germany) and formic acid (98%, Merck, Darmstadt, Germany) in a weight ratio of 2:1 to acquire a PCL solution of 14 wt.% concentration. After mixing, the solution was stirred at room temperature for 24 h. The electrospinning process was performed on the INOSPIN Mini device (Inocure, Praha, Czech Republic) based on needle spinning. The electrospinning conditions have been optimized by Kupka et al. [51] and adapted to the INOSPIN Mini device. The applied voltage was +40 kV on the needle and −10 kV on the collecting electrode. The electrode distance was 155 mm. The needle used has a diameter of 16 G, and the flow of the polymer solution was 0.35 ml/min. The volume of polymer solution used for one PCL mat was 3 ml. The nanofibers (NFs) were collected on a polypropylene nonwoven textile placed on the collecting electrode – a rotating cylinder with a rotation speed of 20 rpm. PCL NF mats were coated with amine or carboxyl plasma polymers (PPs) by plasma-enhanced chemical vapor deposition (PECVD) in low-pressure capacitively coupled radio frequency (RF) discharge.

2.2.2. Amine plasma polymer deposition

Amine PPs were deposited in a stainless steel parallel plate reactor (R2), the scheme of which has been described in detail elsewhere [45,52]. The bottom electrode, 420 mm in diameter, was capacitively coupled to an RF generator working at a frequency of 13.56 MHz. The deposition mixture of cyclopropylamine (CPA, 98%, Merck, Darmstadt, Germany) and Ar (99.999%, Air products, Brno, Czech Republic) was fed into the chamber through a grounded upper showerhead electrode, 380 mm in diameter. The distance between the electrodes was 55 mm. The Ar flow rate was set to 28 sccm, whereas the flow rate of CPA was held at 2 sccm. The power was 100 W, and the discharge was operated in the pulsed mode using a duty cycle of 33% and a repetition frequency of 500 Hz at a pressure of 50 Pa. The deposition time was set to 47 min to achieve a PP coating thickness of 250 nm on the Si substrate. Before the deposition, NFs were clean-sputtered in an Ar discharge using the same settings as for the deposition for 5 min. The deposition conditions were selected to prepare an amine PP thin film with optimal stability and functionality based on previous studies [48,53].

2.2.3. Carboxyl plasma polymer deposition

The carboxyl PPs were deposited in a UHV stainless-steel reactor (R4) with parallel plate electrodes, 210 mm in diameter, and other characteristics identical to the above-described larger R2 reactor from the deposition mixture of ethylene (C_2H_4) and carbon dioxide (CO_2). Deposition conditions were chosen according to the procedure previously optimized on Si substrates for improved stability and surface functionality [54] and adapted for the R4 reactor [55]. The pressure was kept at 10 Pa and the C_2H_4 gas flow rate was held constant at 4 sccm. First, a highly crosslinked base layer was prepared at the RF power of 70 W and the CO_2/C_2H_4 flow rate ratio 2:1. Then, a less crosslinked layer with more functional groups was deposited on the top at 20 W and the CO_2/C_2H_4 ratio of 6:1 by enhancing the plasma oxidation process. The deposition time for the crosslinked layer was 5 min and for the functional layer 1 min to obtain a thin film of 80 nm in total on the Si substrate. Before the deposition, NFs were clean-sputtered in an Ar discharge at 50 W and 10 Pa for 5 min.

2.2.4. Oxygen treatment

In addition, PCL NFs were also treated with an oxygen discharge in the R4 reactor. Oxygen flow rate was set to 10 sccm at a pressure of 50 Pa. The discharge was initiated at 20 W for 2 min.

2.3. Material characterization

2.3.1. Dynamic light scattering

The hydrodynamic particle size, polydispersity index (PDI), and zeta potential of the particle in colloids/suspensions were assessed by dynamic light scattering (DLS) using a Malvern Zetasizer Nano-ZS90 (UK). To prepare the samples, 200 μl of particle colloids/suspensions was diluted with 1800 μl of water, resulting in a total volume of 2000 μl. Hydrodynamic diameter and polydispersity index (PDI) were measured using a plastic cuvette, while zeta potential was evaluated with a Malvern Zeta potential capillary cell (DTS1070). Each sample was analyzed at a backscatter angle of 173° at a temperature of 25 °C, allowing for a 120-second equilibration prior to measurements. Each sample underwent three separate analyses consisting of 12 to 15 measurement runs per repetition.

2.3.2. Water contact angle

The water contact angle (WCA) values were measured on nanofibrous mats by the sessile drop (3 μl of demineralized water) method and evaluated by SeeSystem 7.0. (Advex Instruments, Brno, Czech Republic) software calculating the WCA based on three-point interpolation of the drop height and width from snapshots taken by a CCD camera. The drop snapshots were captured with a ~0.2 s delay after the droplet touched the surface to ensure a correct comparison because the shape of the water droplet changed rapidly after the contact. The mean WCA and its standard deviation were estimated from ten droplet measurements.

2.3.3. X-ray photoelectron spectroscopy

X-ray photoelectron spectroscopy (XPS), used for the surface chemical characterization (information depth from the maximum of 5 nm), was carried out using an Axis Supra (Kratos Analytical, Manchester, UK) spectrometer with an X-ray monochromated source (combined Al/Ag anode). Spectra were acquired with a charge neutralization in overcompensated mode to avoid differential charging of samples. The binding energies were corrected by shifting the hydrocarbon component CH_x to 285.0 eV. The elemental atomic percentage was quantified from the high-resolution spectra of each element taken at the pass energy of 20 eV. The high-resolution O1s and C1s spectra were fitted by CasaXPS software version 2.3.19 (Casa Software Ltd, Teignmouth, UK) after subtracting the Shirley-type background to obtain individual components. The components were Gaussian–Lorentzian (G-L) shaped with a fixed G-L percentage of 30%. The full width at half maximum was between 0.9–1.3 eV and 1.1–1.7 eV for all carbon and oxygen components, respectively. The values of the binding energies for various oxygen and carbon environments were taken from Beamson and Briggs [56] if not stated otherwise. To carry out the XPS of lignin particles, 100 μl of the as-received colloids/suspension was dropped on a silicon substrate and dried. Lignin MPs in the form of powder were glued to the conductive tape.

2.3.4. Scanning electron microscopy

The surface morphology was studied using an SEM LYRA3 (Tescan, Brno, Czech Republic) microscope in secondary emission mode (10 kV acceleration voltage, 4–6 mm working distance). The micrographs were acquired with a resolution of 1024 × 1024 pixels. Before imaging, the samples were coated with a 5–10 nm thick gold film deposited by radiofrequency magnetron sputtering (Leica ACE 600, Leica Microsystems, Wetzlar, Germany) to eliminate the charging of the sample surface during imaging. To carry scanning electron microscopy (SEM) analyses of lignin particles, 100 μl of the as-received colloids/suspension was dropped on a silicon substrate and dried. Lignin MPs in the form of powder were glued to the conductive tape.

2.4. Immobilization and release of lignin nano/microparticles

Based on preliminary experiments (see Section S3.1 for details), the wet process was employed to immobilize lignin particles. Colloids/suspensions of lignin particles with different mass concentrations were used based on supply as follows: 15NPs – 0.8 mg/ml, 50NPs – 0.5 mg/ml, 300NPs – 2.5 mg/ml, and MPs – 3.8–6.5 mg/ml. The nanofibrous mats after immobilization were washed to evaluate how firmly the lignin particles stick to the NF mats.

For XPS and SEM analyses, NF mats together with supporting spunbond (to ensure easy manipulation) were cut into squares of 1 × 1 cm^2, dipped in 1 ml of the lignin colloid/suspension for a short time (~5 s), let soak up, pulled out, and let dry. To differentiate the effect of only water immersion from lignin immobilization on PCL references, the pristine and plasma-modified nanofibrous mats were immersed in deionized water and allowed to dry. These samples are labeled 'rinsed' throughout the text. The NF mats with immobilized lignin were immersed in deionized water, stirred for ~10 s, pulled out and let dry.

For UV–Vis spectroscopy (see the method details below), nanofibrous mats were cut into squares of 1.5 × 1.5 cm^2, peeled from the supporting spunbond, fixed into CellCrown™ inserts (Scaffdex, Finland) to enable fine manipulation, dipped in 2 ml of lignin colloids/suspensions for ~5 s, let soak up, pulled out, and let dry in the Petri dish. Afterwards, the nanofibrous mats with immobilized lignin were immersed in deionized water and shaken using a Heidolph Vibramax 100 shaker for 24 h.

2.4.1. UV/Vis measurements of lignin immobilization and release

Lignin concentrations in colloids/suspensions were measured using UV–Vis spectroscopy (UV/Vis/NIR spectrophotometer Jasco V-770 for 15NPs, 50NPs and MPs, and Tecan Spark Cyto plate reader for 300NPs), utilizing lignin absorption peak at 283 nm [57]. For each type of particle, 10–15 colloids/suspensions with known concentrations were used to obtain a linear calibration curve (see Fig. S2).

The immobilized amount of lignin was calculated as the difference between the initial lignin amount in the colloid/suspension and the amount remaining there after the immobilization on the NF mat. However, some lignin was also lost on the CellCrown inserts and Petri dishes, which were used as tools during immobilization. These losses were estimated by carrying out the immobilization procedure without nanofibers, rinsing the CellCrown inserts and Petri dishes, and measuring the lignin amount in the obtained colloids/suspensions. The immobilization results were corrected by subtracting the estimated losses, which were calculated for each particle and modification type. The amount of lignin released into water after washing the NF mats with lignin was quantified directly using the calibration curves for each type of particle.

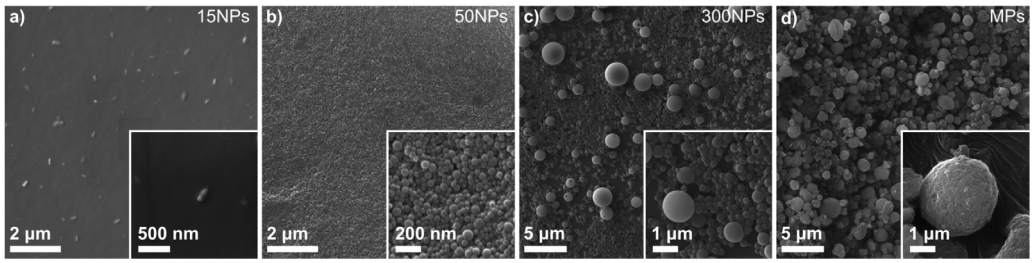

Fig. 1. SEM micrographs of lignin particles: (a) 15NPs, (b) 50NPs, (c) 300NPs and (d) MPs. Figure insets show high-resolution images of the particles' details.

3. Properties of lignin nano/microparticles

3.1. Characterization of lignin nano/microparticles

Properties of lignin particles are summarized in Table 1. Averaged diameters were calculated based on the evaluation of SEM micrographs (illustrative images in Fig. 1). 15NPs and 50NPs particles were prepared by the solvent-shifting method using water as a nonsolvent (details in Section 2.1). Using DMSO as a solvent, the lignin solution self-assembled through a mechanism resembling spinodal decomposition. Bicontinuous structures emerged that coarsen to numerous primary particles, from which smaller particles were deposited onto bigger ones through Ostwald ripening [49]. This process allowed the formation of exceptionally small particles with an average diameter of 15 nm (15NPs, Fig. 1a). The utilization of THF solvent resulted in particles with an average diameter of 50 nm (50NPs) grown by a typical nucleation & growth mechanism, specifically multiple nucleations and Ostwald ripening growth [49]. The 50NPs particles looked like regular spheres with a narrow size distribution, which did not tend to agglomerate into larger clusters (Fig. 1b). Nanoparticle colloids exhibited low polydispersity indexes (PDI, Table 1), confirming monodisperse solutions, which were stable for months.

For the first time, we synthesized 300NPs particles using 1% acetic acid solution as a nonsolvent and THF as a solvent with again a regular spherical shape and an average diameter of 320 nm. However, the size distribution was broad (see Fig. S3). The diameters ranged widely between 150 nm and 800 nm, but even particles with 7 µm diameter were present, as evidenced by the micrograph in Fig. 1c. The larger size of 300NPs can be attributed to the use of an acetic acid solution during solvent shifting, which can protonate carboxylic groups in lignin, thereby promoting the aggregation of smaller particles into larger ones. Moreover, some 300NPs were hollow, in contrast to the 50NPs.

MPs particles prepared by spray drying were found to be microparticles with diameters ranging from 1200 to 2200 nm. They formed irregular oval or doughnut-like agglomerates. Since MPs were prepared from 50NPs by spray-drying, individual nanoparticles of ~50 nm diameter can be distinguished after sufficient magnification (Fig. 1d). As a complementary method to SEM, DLS was employed to determine lignin particle sizes. Hydrodynamic sizes (Table 1) are larger compared to SEM's diameters due to particles' solvation during measurement.

The chemical composition of all lignin particles was similar, consisting of carbon, oxygen, nitrogen, and sulphur. The sulphur did not originate from lignin itself, but it is a remnant of the lignin extraction method — the kraft process. The sulphur content for bulk analyses of kraft lignin was around 2 at.% (see Section 2.1), but prepared lignin particles showed only 0.6 at.% of sulphur on their surface, suggesting that the synthesis also had a purification effect on lignin. Lignin particles consisted, on average, of 77.1 at.% of carbon and 22.3 at.% of oxygen. 15NPs and 300NPs showed a bit higher amount of oxygen compared to the others (50NPs and MPs). However, a weak silicon signal from the underlying substrate used for XPS analysis was also detected for 15NPs and 300NPs samples. Since the silicon substrate is covered with a native oxide layer (a few nanometers in thickness), oxygen content for those lignin particles can be slightly overestimated. Therefore, the average lignin composition was calculated based on only values for 50NPs and MPs whose spectra were unaffected by non-related material.

Typical C1s spectrum of lignin with identified chemical bonds can be found in Fig. S4. In general, lignin chemical structure consists of methoxylated phenylpropane units, generated from three aromatic alcohols (monolignols), *p*-coumaryl, sinapyl, and coniferyl alcohols. The proportion and type of monolignols fluctuate considerably in lignin from different plant species. Kraft lignin used in this work originated from softwood, which is mainly composed of coniferyl alcohol with traces of *p*-coumaryl alcohol [1]. Lignin forms a highly branched structure in which both aliphatic and phenolic hydroxyls as well as carboxylic groups (identified also by XPS — Fig. S4) acquire a negative surface charge when immersed in a water environment. Therefore, all prepared lignin particles exhibited negative zeta potential between −33 and −40 mV (Table 1). High negative (or positive) surface charge prevents particles from agglomeration by electrical double layer repulsion, which translates into good stability of NP colloids [49]. Although a differing zeta potential could be expected in the case of 300NPs due to protonation of lignin carboxyl groups during the synthesis, the traces of acetic acid were removed through dialysis. Hence, a return to a deprotonated state can follow, explaining the comparable zeta potential value to those of other lignin particles.

3.2. Antimicrobial effect of lignin particles

Native lignin, besides its structural role in plants, also prevents the degradation of carbohydrates by inhibiting the activity of bacteria and fungi [4]. This lignin property can be exploited in further bioapplications as a natural alternative to antibiotics. Therefore, the antimicrobial activity of all lignin particles was tested in suspensions against gram-negative *E. coli* and the calculated ALR (Eq. (1)) values are given in Fig. 2. Surprisingly, only 300NPs exhibited a strong inhibition effect with the ALR of 8.4, starting at a concentration of 0.4 mg/ml determined as the minimum inhibitory concentration (MIC). Considering the detection limit of the plating method, which is ~10 CFU/ml, the corrected ALR value for 300NPs is >7.4.

Smaller (15NPs and 50NPs) and larger (MPs) lignin particles did not influence bacteria growth at all, and bacteria prospered similarly to the control. Neither once nor twice higher concentrations (0.7 and 1.4 mg/ml) of smaller particles caused any bacteria inhibition; on the contrary, bacteria growth was promoted slightly. Even a rapid increase of MPs concentration to 10 mg/ml did not help to achieve any antimicrobial effect against *E. coli*. On the other hand, MPs (10 mg/ml) inhibited the growth of gram-positive *S. aureus*. Since MPs exhibited the ALR of 3, we can conclude that a concentration of 10 mg/ml is close to the MIC for *S. aureus*.

Even though small lignin NPs (<90 nm) have already been shown to inhibit more sensitive gram-positive *S. aureus*, at the same time, they displayed a lower effect on more resilient gram-negative strains [58] or were ineffective at all against *E. coli*, using a similar concentration as

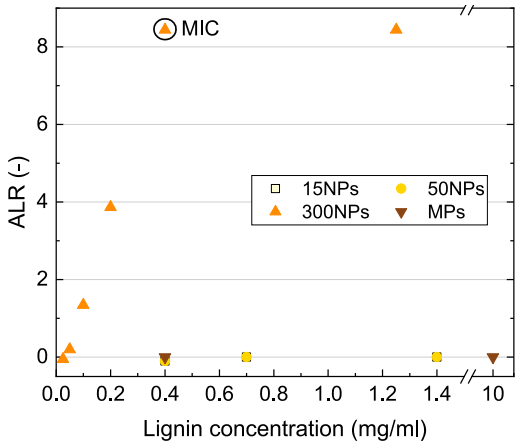

Fig. 2. Antimicrobial log reduction (ALR) for lignin 15NPs, 50NPs, 300NPs and MPs in suspension cultivated with *E. coli*. ALR was determined after 24 h of cultivation. Minimum inhibitory concentration (MIC) for 300NPs was assessed as 0.4 mg/ml.

in our work (0.1 mg/ml) [59] or even much higher (35 mg/ml) [60]. Although other authors reported an antimicrobial effect of small lignin NPs against *E. coli* [61] or other gram-negative bacteria [3], the used concentrations were much higher (at least 40 mg/ml), to achieve an ALR of at least 3 and lower.

The effect on gram-negative bacteria improved with a bigger particle size; lignin NPs of 215 nm showed higher bacteriostatic effect on *E. coli* and *Salmonella enterica* than 75 nm [62]. Lignin NPs up to 500 nm inhibited the growth of both gram-positive as well as gram-negative strains using concentrations of 2–7 mg/ml [63,64]. As was shown by Kim et al. [65], larger particles (up to 800 nm, 3 mg/ml) were still effective against gram-positive *S. aureus*, reaching the ALR of 4. However, with a growing size, the effect on gram-negative bacteria starts to diminish again, as was observed by Morcillo-Martín et al. [66] for particles of ~1000 nm; *S. aureus* was inhibited using a similar concentration as in the case of Kim et al. [65] (2.25 mg/ml) whereas 9 mg/ml was needed to stop the growth of *E. coli*, which corresponds to our findings for slightly larger MPs. We can argue that the sizes of MPs and bacteria (*S. aureus* and *E. coli*) are comparable, which minimizes the contact area between them. Therefore, the possible antimicrobial action is also highly reduced.

ALR > 7.4 achieved in our experiments for 300NPs and *E. coli* is exceptional compared to published results. The antimicrobial activity can be partly related to their medium size (larger compared to 15NPs and 50NPs but smaller than MPs), which can be considered optimal. However, the mechanism of lignin antibacterial activity has not yet been fully elucidated. It is usually correlated with the presence of methoxy and phenolic hydroxyl [3] groups in lignin structure. Polyphenolic compounds may damage bacterial membranes by generating oxygen reactive species, *i. e.,* hydrogen peroxide [67]. Using lignin as an antibacterial agent might benefit from these nonspecific modes of action, reducing possible resistance development in bacteria. Furthermore, lignin in NP form can introduce other modes of action, combining penetration inside the cell, resulting in increased levels of oxidative stress and decreased metabolic activity, and adherence to bacterial membrane, followed by intercalation, which eventually causes membrane disruption and cell lysis [4].

3.3. Cytotoxicity of lignin particles

When aiming for bioapplications and assuming lignin particle contact with living tissues, not only the antimicrobial effect, but also cytocompatibility must be considered. However, authors scarcely investigate both at the same time. Only Freitas et al. [62] from the summary above were concerned about the cytotoxicity of their lignin NPs. Here, cell proliferation *in vitro* helped differentiate between cytocompatible and cytotoxic levels of lignin by adding lignin particle suspensions with various concentrations (0.01–1.4 mg/ml) into the cell culture media. Keratinocytes (HaCaT) and human fibroblasts (LF) were chosen for testing as representatives of skin cells and cells necessary for wound healing, respectively. The proliferation results are shown as values relative to the control without adding lignin particles in Fig. 3.

We can notice that small amounts (up to 0.05–0.1 mg/ml) of smaller particles (15NPs and 50NPs) can even promote the proliferation of both types of cells. Smaller particles were better tolerated by the tested cells in general; 50NPs at the concentration of 1.4 mg/ml did not reduce cell viability by more than 50% for LF cells and did not harm HaCaT cells. Similarly, no cytotoxic effect was reported for low concentrations (up to 10 μg/ml, NPs of ~112 nm) for HaCaT cells [68], and only a slight decrease in human embryonic kidney cell viability up to 20% was observed for a higher concentration (1 mg/ml, NPs, ~130 nm) [69]. In contrast, Zhang et al. [70] also tested small NPs (65–90 nm) at similar concentrations as in our work (0.01–0.64 mg/ml) with hepatocytes cells, and all concentrations, except for 0.01 mg/ml, showed to be cytotoxic, although the lignin transformation into NP form drastically reduced toxicity compared to the dissolved form.

300NPs had the most harmful impact; they caused the detachment followed by death of almost all cells at concentrations starting with 0.2 mg/ml (Fig. S5). The mechanism of cell death was studied using LF cells and a caspase 3/7 assay (for more details see Section S2), giving a positive staining in case of the apoptotic process activation. However, the cell death proved to be not caspase-specific (Fig. S6) and most likely is caused by necrosis [71]. Larger NPs (~225 nm) prepared by Yu et al. [72] induced a comparable effect on mouse fibroblasts, whose viability was reduced almost to zero using a concentration of 0.5 mg/ml and higher after 3-day exposure. However, they proved the effect was time-dependent since all tested concentrations were cytocompatible within the first 12 h of contact. For HaCaT cells, MPs were toxic even at the lowest used concentration of 0.04 mg/ml. On the other hand, LF cells withstood the presence of MPs up to 0.4 mg/ml without a significant negative effect.

We can conclude that the harmful effects on both cells and gram-negative bacteria are size and concentration-dependent. Small lignin NPs (up to 110 nm) do not damage either of them even at relatively high concentrations around 1 mg/ml. To kill gram-negative bacteria, an excessive amount of small lignin NPs (tens of mg/ml) is needed. On the other hand, safe concentrations of small lignin NPs may be effective against more susceptible gram-positive bacteria. NPs larger than 200 nm also start to inhibit gram-negative bacteria using a concentration below 1 mg/ml. However, such a concentration already kills cells efficiently. With a further growing size (>1000 nm), the harmful effect on both cells and bacteria diminishes again. Therefore, larger NPs (200–1000 nm) seem to be a reasonable candidate for an antimicrobial agent, but finding a compromise between antimicrobial and cytocompatible concentration proved challenging and is a subject of further study.

4. PCL nanofibrous mats plasma-modified for lignin immobilization

4.1. Morphology of PCL nanofibrous mats

Pristine nanofibers had an average diameter of (240 ± 10) nm. The mats comprised randomly oriented NFs with sporadically present beads (Fig. 4a; Fig. S7). O_2 treatment had to be carefully tuned to not damage the NF structure since the first attempts resulted in their melting (Fig. S8, melted). Even after optimization, we were not able to avoid harming NFs altogether. As evident from the SEM micrograph in Fig. 4b and Fig. S8, the O_2 plasma treatment etched the NF surface, causing its roughening. Since the uppermost layer of NFs was only enriched by

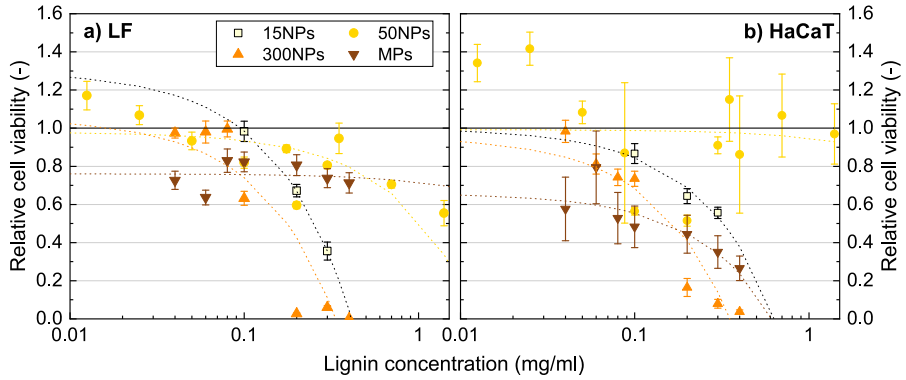

Fig. 3. Proliferation of LF (a) and HaCaT (b) cells cultivated with the addition of lignin particles with different concentrations to culture media. Cell proliferation was assessed by ATP assay 2 days after seeding and expressed as a relative value to the control (cell medium without lignin addition). The error bars represent the standard deviation of the mean. The lines representing the linear fits of the data were added to guide the eye.

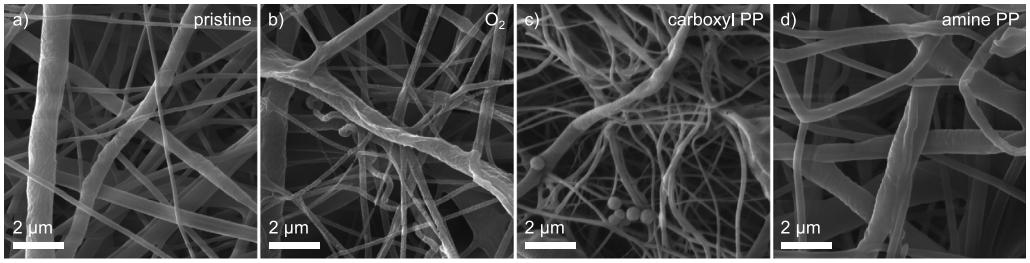

Fig. 4. SEM micrographs of references: (a) pristine, (b) O_2-treated, (c) carboxyl-PP-coated, (d) amine-PP-coated PCL NFs. View field of 10 µm.

functional groups after O_2 treatment, the thickness of NFs remained unchanged ((230 ± 20) nm).

NFs coated by amine PPs (Fig. 4d, Fig. S9) or carboxyl PPs (Fig. 4c, Fig. S10) were visually indistinguishable from pristine NFs. The morphology of the NFs remained preserved and was neither influenced nor damaged by the interaction with the plasma discharge. The diameter of NFs increased by 90 and 30 nm for amine and carboxyl PPs, respectively. In both cases, the thicknesses of thin films on the nanofibrous non-planar substrate were roughly 5× lower than the thickness on a flat silicon substrate (250 and 80 nm, respectively — see Section 2.2). Interestingly, particles of (460 ± 10) nm in diameter were created during carboxyl deposition and are occasionally recognizably attached to NFs (Fig. 4c). Moreover, carboxyl-PP-coated NFs exhibited pronounced wrinkled morphology, which is not typical for other coatings, *i. e.,* amine PP coating, or pristine NFs. Since the wet process was employed to immobilize lignin particles (see Section 2.4 for details), water immersion's influence on reference NFs must be considered and differentiated from the effect of lignin immobilization. However, the appearance of rinsed references was not altered by contact with water, as confirmed by SEM (Fig. S11).

4.2. Chemical composition of PCL nanofibrous mats

The chemical compositions of all references, pristine and plasma-modified PCL NFs, as well as reference NFs after water immersion, are given in Fig. 5 (initial and rinsed).

4.2.1. Pristine PCL nanofibrous mats

Pristine NFs consisted of 25.5 at.% of oxygen and 71.2 at.% of carbon. Besides, small amounts of phosphorus (2.4 at.%) and potassium (0.9 at.%) were present. This contamination of PCL NFs is probably caused by spunbond supporting textile, which also contains phosphorus and potassium [73]. We suppose some potassium phosphate ($K_xH_yPO_4$) is used while manufacturing the spunbond textile, which slightly diffuses into NFs.

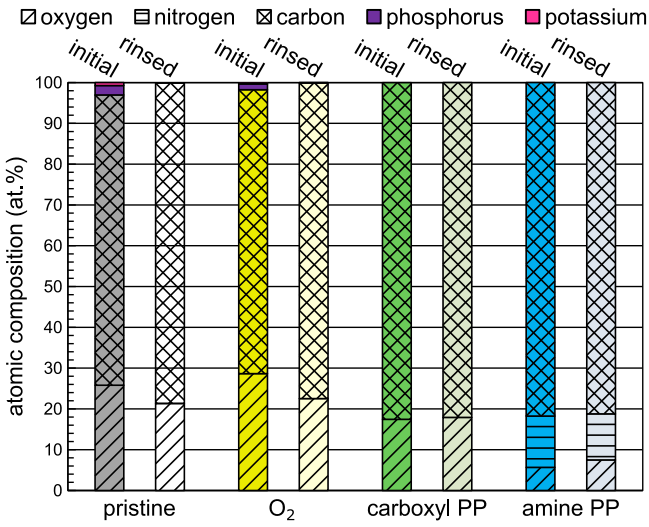

Fig. 5. XPS chemical composition of references: pristine and plasma-modified PCL nanofibrous mats as-prepared (initial) and after immersion into water (rinsed).

The phosphorus and potassium contamination disappeared after washing the NFs. This loss was accompanied by an oxygen decrease from 25.5 at.% to 21.2 at.%. However, it is not probable that oxygen from PCL is lost. Instead, we are convinced that the oxygen missing after washing originated from the washed-out potassium phosphate, which is supported by the change in high-resolution spectra of the O1s peak (Fig. S12). While the fitting model of the initial O1s peak contained an additional component at 531 eV that can be associated with PO_4^{3-}, only two components at 532.2 eV (O=C) and 533.5 eV (O–C), typical for PCL [56], with a ratio of 45:55, can be easily differentiated in the case of rinsed NFs. Therefore, the actual PCL

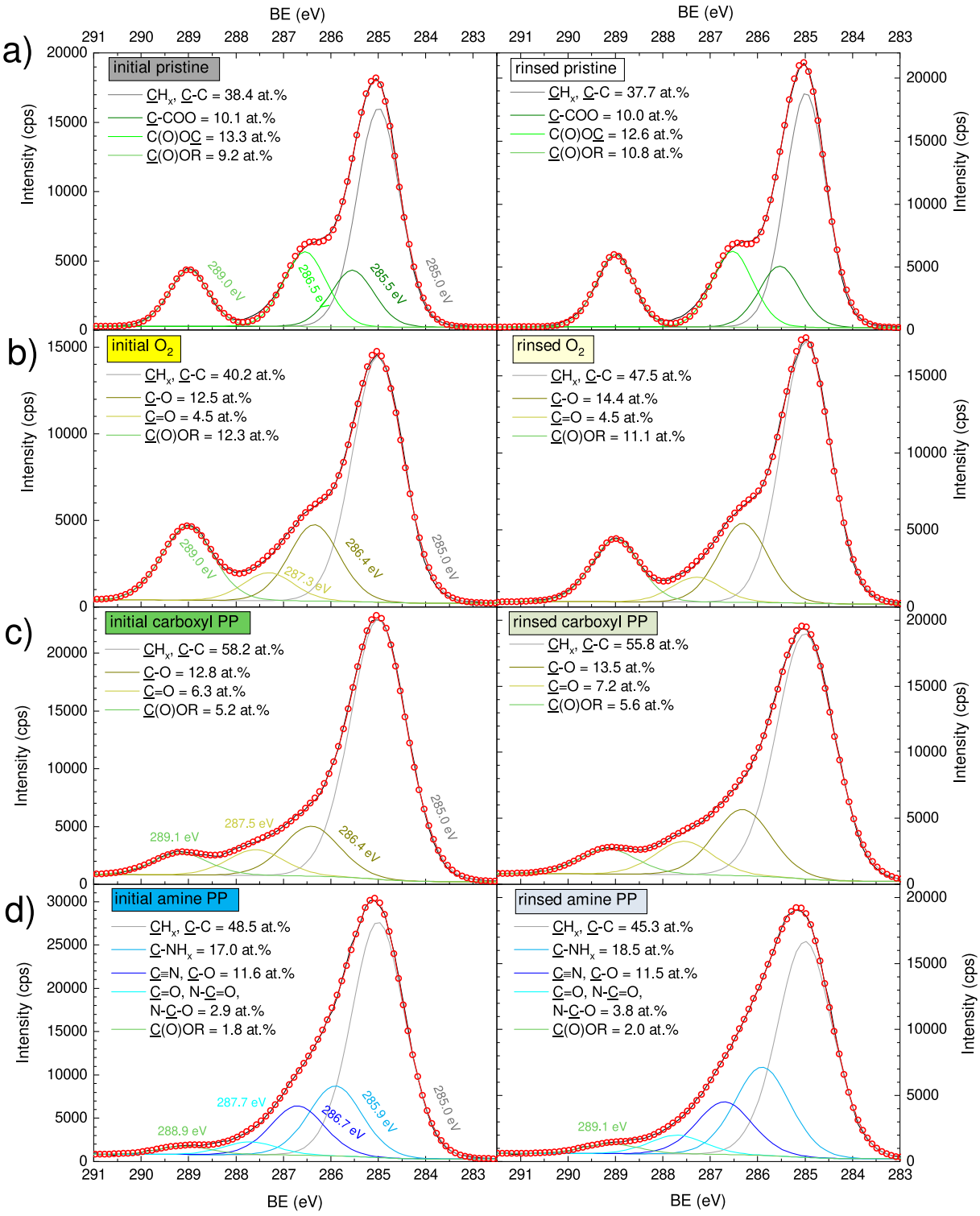

Fig. 6. Chemical bonds identified based on fitting of XPS C1s high-resolution spectra of initial (left column) and rinsed (right column) PCL nanofibrous mat: (a) pristine, (b) after O_2 plasma treatment, (c) coated by carboxyl PP, (d) coated by amine PP.

NFs composition corresponds to pristine NFs after washing (Fig. 5) – 21.2 at.% of oxygen and 78.6 at.% of carbon.

Wettability can also support this explanation. Although the pristine NFs are hydrophobic given their nature [74], the measured water contact angle (WCA) was only 62.6° ± 1.6° (Fig. S13), probably caused by phosphate contamination. After rinsing, WCA reached an expected hydrophobic value of 120.9° ± 0.8° (Fig. S13).

4.2.2. Oxygen-plasma treated PCL nanofibrous mats

PCL NFs treated in oxygen plasma had 3 at.% higher amount of oxygen than pristine NFs (Fig. 5, initial), indicating successful grafting of additional oxygen-containing functional groups. Although the difference in chemical composition is small, the O_2 treatment had a striking effect on the wettability. The O_2-plasma-treated NFs showed hydrophilic behavior with a WCA of 31.4° ± 1.5° (Fig. S13). Since only a monolayer of oxygen-containing groups was formed on the NF surface,

most of the XPS signal comes from the NFs themselves. In contrast, WCA measurement is more surface-sensitive, primarily reflecting the uppermost surface. Hence, low WCA indicates a surface rich in polar oxygen-containing groups oriented toward the surface, whose total atomic concentration is yet too small to make a larger difference from the substrate by XPS.

However, the contribution of phosphate contamination to the composition still needs to be kept in mind because oxygen treatment results in only grafting oxygen-containing groups on the surface, and P and K were still detected (1.4 at.% and 0.3 at.%, resp.). After immersion of the O_2-plasma-treated mats into the water, the oxygen surface content dropped by about 6 at.%, which is only a 1 at.% higher than the rinsed pristine mats. Since P and K are not present after rinsing, the oxygen loss can be, on that account, mainly ascribed to washed-out potassium phosphate and partly to vanished oxygen-containing groups from treatment.

Nevertheless, some functional groups from treatment remained even after rinsing because the components of the C1s peak differed from those of rinsed pristine PCL (Fig. 6a and b). The C1s peak was fitted with the four components: aliphatic hydrocarbon groups (CH_x, C–C) at 285.0 eV, hydroxyl/ether (C–O) at 286.4 eV, aldehyde/ketone (C=O) at 287.3 eV, and carbon in carboxyl/ester group (C(O)OR) at 289.0 eV [56]. In contrast, pristine PCL contains, except for hydrocarbon and ester groups, components at 285.55 eV (C–C(O)OR) and at 286.5 eV (CO(O)C). Moreover, the wettability did not return to hydrophobic behavior; the rinsed O_2-treated NFs stayed mildly hydrophilic ($85.1° \pm 6.7°$, Fig. S13). On the other hand, the carboxyl/ester group signal of O_2-treated NFs likely originated from the PCL substrate rather than from the treatment, since they both contained similar amounts of these groups after rinsing. Consequently, carboxyl/ester groups may not contribute to functionalization in this case.

4.2.3. Carboxyl plasma polymer coated PCL nanofibrous mats

Since carboxyl-PP-coated NFs contained 17.5 at.% of oxygen, about 8 at.% less than pristine NFs (Fig. 5, compared to the initial state), we can be positive that the measured signal came from a carboxyl PP thin film, which successfully covered the surface of NFs. The C1s peak (Fig. 6c) can be fitted with the same model as for O_2-plasma-treated NFs but the aldehyde/ketone component had to be shifted to higher energies (from 287.3 eV to 287.5 eV) [54,55]. Comparing modifications forming oxygen-containing groups, carboxyl PP coating contained significantly more aliphatic hydrocarbon groups and fewer carboxyl/ester groups than O_2-treated NFs, suggesting a higher degree of functionalization for the latter. However, the carboxyl/ester groups in O_2-treated NFs were ascribed to the underlying PCL substrate (as mentioned above). Therefore, the degree of functionalization for carboxyl-PP-coated NFs was higher with ~26 at.% functionalities in contrast to ~19 at.% for O_2-treated NFs.

Carboxyl PP coating proved invariant under water immersion because rinsing did not alter its composition. Despite the abundant presence of polar functional groups, carboxyl-PP-coated NFs were hydrophobic with a WCA of $118.6° \pm 1.2°$ (Fig. S13), similar to rinsed PCL. Since carboxyl PP, as a flat film, is hydrophilic [55], the hydrophobic nature of carboxyl-PP-coated NFs has to be related to their structure.

4.2.4. Amine plasma polymer coated PCL nanofibrous mats

The composition of PCL NFs coated with amine PP included (12.6 ± 0.4) at.% of nitrogen, proving the incorporation of nitrogen-containing functional groups. ~6 at.% of oxygen was also present due to the post-plasma oxidation of amine PPs after exposure to ambient air (Fig. 5, initial). As a consequence, amine PP thin films incorporated both nitrogen and oxygen-containing functional groups, as evident from the fitting of XPS C1s high-resolution spectra (Fig. 6d). The C1s signal was composed of aliphatic hydrocarbon groups at 285.0 eV, amino groups bonded to carbon (C–NH_x) at 285.9 eV, nitrile and ether groups (C#N, C–O) at 286.7 eV, aldehyde/ketone or amide groups (C=O/N–C=O/N–C–O) at 287.9 eV, and ester/carboxyl groups at 288.9 eV. Since the positions of some carbon–nitrogen and carbon–oxygen bonds overlap, groups with close binding energies were coupled in one component. Therefore, C–O and C=O were slightly shifted to higher energies, by 0.1–0.3 eV, compared to the modifications incorporating only oxygen-containing groups. The identified functional groups are consistent with our previously published results for amine PP [48,55,73].

After rinsing, amine PPs oxidized even more, increasing oxygen concentration by 2 at.% at the expense of nitrogen, which translated into a drop of amino groups and growth of aldehyde/ketone and amide groups, as well as a slight shift of CO(O)R group to higher energies (+0.2 eV). Amine-PP-coated NFs were slightly hydrophilic with a WCA of $89.9° \pm 3.0°$ (Fig. S13) [48].

5. Efficiency of lignin particle immobilization on PCL nanofibrous mats

5.1. Morphology of PCL nanofibrous mats after lignin immobilization

We investigated the immobilization of all types of lignin particles (15NPs, 50NPs, 300NPs and MPs) through the wet process (see Section 2.4 for details) on pristine, O_2-plasma-treated, and amine and carboxyl-PP-coated PCL NFs. Micrographs of PCL NF mats after lignin immobilization are summarized in Fig. 7; pristine and plasma-modified NF mats for comparison can be found in Fig. 4. The most challenging appeared to be the binding of small particles, *i. e.,* 15NPs and 50NPs. Both types visibly homogeneously covered the whole surface of individual fibers only on amine-PP-coated NFs. In similar numbers, 15NPs can also be distinguished on pristine NFs. On carboxyl-PP-coated NFs, small particles are difficult to spot, since they were present more infrequently and were localized. (For better resolution, see Fig. S15 and S16 with highlighted 15NPs and 50NPs, respectively.) Moreover, the wrinkled morphology of carboxyl-PP-coated NFs could hinder the recognition of small particles. Except for random scarce particles, the immobilization on other NFs was not confirmed by SEM.

On the other hand, the presence of the larger 300NPs and MPs was detected on all tested NF mats. Larger particles were too big to cover individual fibers. In the case of 300NPs, particles either stuck to the surface of the nanofiber mat or formed clusters (mainly in the lower layers of NFs rather than on the surface). MPs covered the top surface of NFs and were also present inside the mat. They kept their spherical or doughnut-like shape; some smaller fragments composed of nanoparticles (in the size of tens and hundreds of nanometers) can be occasionally noticed on individual nanofibers. Visually, the immobilization on pristine NFs seems to be the most effective for 300NPs, and there is no apparent difference among immobilization conditions in the retention of MPs. To achieve moderate lignin densities on NF mats, concentrations of immobilization suspension were at least 3× higher (2.5 and 3.8–6.5 mg/ml for 300NPs and MPs, respectively) compared to 15NPs and 50NPs; otherwise lignin binding was negligible (see Fig. S17).

5.2. Chemical composition of PCL nanofibrous mats after lignin immobilization

To validate visual assessment based on SEM, XPS was employed as a complementary method to quantify lignin binding. After the lignin immobilization, some of the NFs randomly showed a minor concentration of sulphur (<0.5 at.%). However, a trace amount of the element alone is insufficient to prove or disprove successful immobilization with certainty based on chemical composition. Except for sulphur, no other elements differentiate lignin particles from NFs. Therefore, we compared O/C ratios after lignin immobilization with rinsed references (Fig. S18) in more detail. As mentioned before, rinsed references were

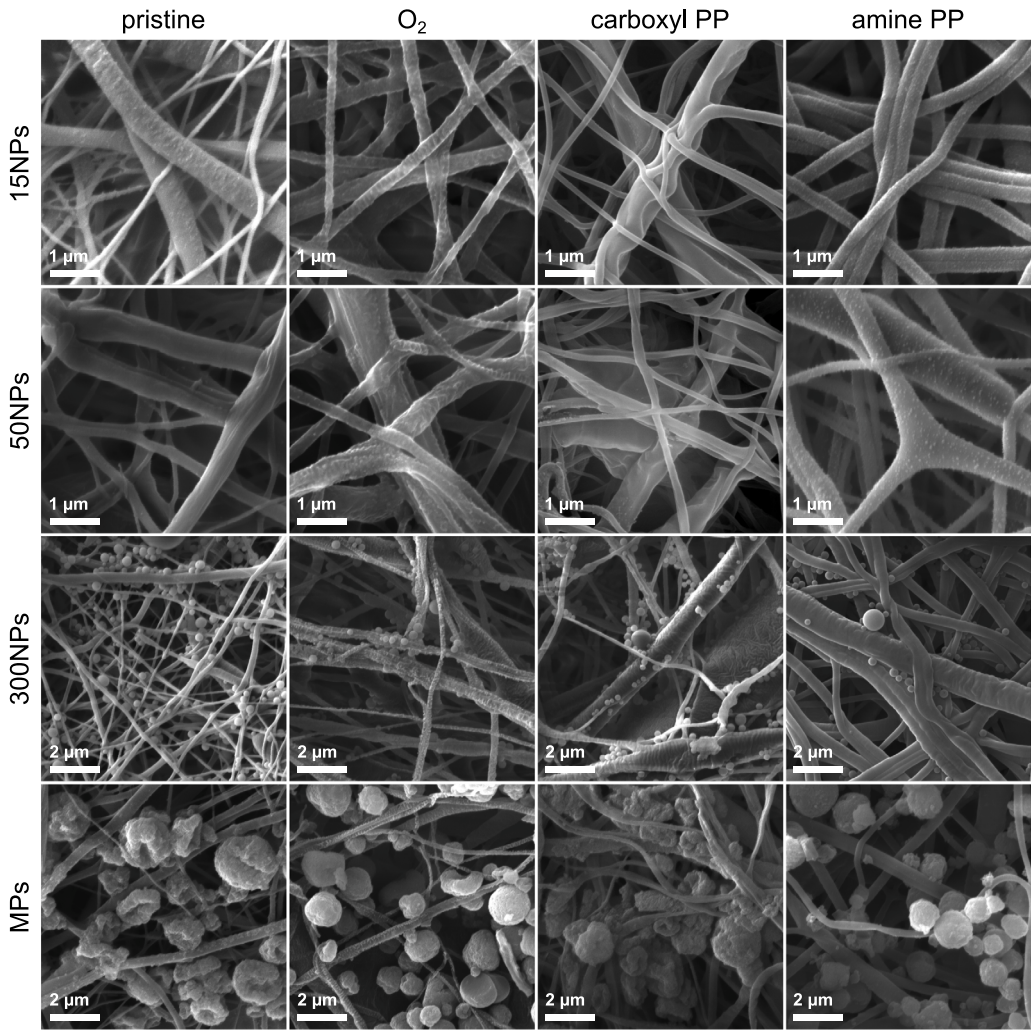

Fig. 7. SEM micrographs of pristine, O_2-treated, carboxyl-PP-coated and amine-PP-coated PCL nanofibrous mats after immobilization of 15NPs, 50NPs, 300NPs and MPs. The initial concentrations of immobilization solution/suspension are given in Section 2.4; MPs were used at concentrations of 3.8, 6.5, 3.8 and 6.5 mg/ml for pristine, O_2 plasma-treated, and carboxyl and amine-PP-coated PCL nanofibrous mats, respectively.

used to distinguish the effect of immobilized lignin from changes resulting solely from water immersion. However, unequivocally evaluating the success rate of lignin immobilization proved challenging due to the small differences in the O/C between lignin (0.289) and rinsed pristine NFs (0.272) and the almost identical composition of lignin (0.289) and rinsed O_2-treated NFs (0.291). Looking closer at the fitting of C1s peaks did not help either since features typical for lignin as π-π^* satellite related to aromatic phenol units and higher binding energy for C(O)OR group (Fig. S4) were not shown in C1s spectra after lignin immobilization, and the fitting models established for individual modifications (Fig. 6) were usable without adjustments also for the NFs after lignin immobilization.

Therefore, we estimated the fraction f of NF area covered by lignin by analyzing the composition changes of all elements simultaneously, taking into account the chemical composition of lignin particles, rinsed reference NF mats, and mats after lignin immobilization:

$$c_{\mathrm{meas},X} = f\,c_{\mathrm{lignin},X} + (1-f)c_{\mathrm{ref},X}\ , \tag{2}$$

where X stands for O, N, or C elements, $c_{\mathrm{meas},X}$, $c_{\mathrm{lignin},X}$ and $c_{\mathrm{ref},X}$ are the atomic concentrations in at.% for X element of the NF mats after lignin immobilization, the lignin particles and the rinsed reference NF mats, respectively. Since the concentrations have comparable uncertainties, f was obtained by a total least squares fit of combined data for all three elements.

The resulting fractions of covered areas are shown in Fig. S19 for pristine and O_2-treated NF mats and in Fig. 8b for amine and carboxyl PPs (columns labeled 'before washing'). The most consistent finding was that amine and carboxyl PP coatings bound all lignin particles in similar amounts; between 20 to 50% of the nanofibrous surface was covered by lignin. The carboxyl PP coating was specific in the immobilization of a high number of 300NPs, which covered 80% of the NF surface. Nonetheless, we could not reliably determine the surface coverage for pristine and O_2-treated NFs because the fitted fractions were either negative (pristine NFs) or the values were higher than 1 and accompanied by errors much larger than the values (O_2-treated NFs) (see Fig. S19). These meaningless outcomes were probably caused by the similarity between the composition of lignin and references that could not be reliably distinguished by XPS due to experimental errors. However, we can draw at least one conclusion from the oxygen concentration of O_2-treated NFs (Fig. 8a). In the case of 300NPs and MPs, the oxygen rise compared to the rinsed reference cannot be explained by anything other than lignin presence.

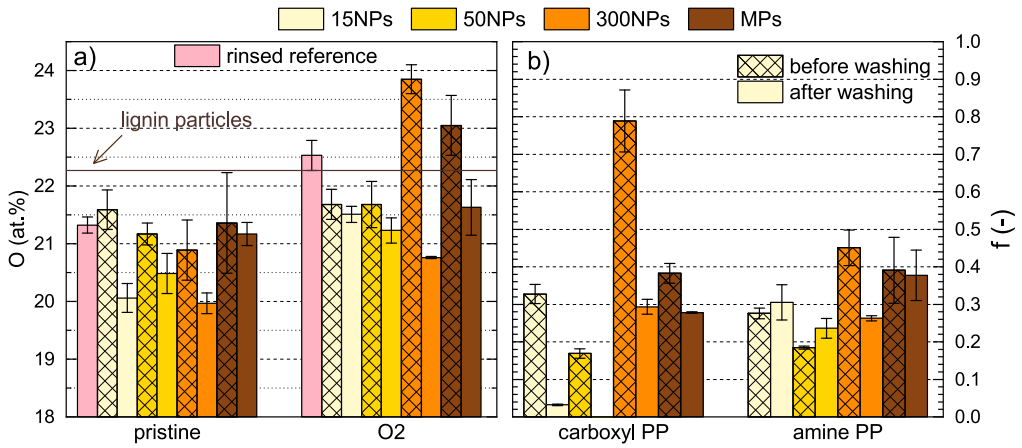

Fig. 8. (a) XPS atomic concentration of oxygen for pristine and O_2 plasma-treated PCL nanofibrous mats after lignin immobilization (before washing) and after lignin immobilization followed by washing (after washing). Rinsed reference is included to ensure proper comparison. (b) Fraction f of PCL area covered by lignin calculated from XPS chemical composition — comparison of amine and carboxyl-PP-coated PCL nanofibrous mats after lignin immobilization (before washing) and after lignin immobilization followed by washing (after washing). The initial concentrations of immobilization solution/suspension are given in part Section 2.4; MPs were used at concentrations of 3.8, 6.5, 3.8 and 5.1 mg/ml for pristine, O_2 plasma-treated, carboxyl-PP-coated and amine-PP-coated PCL nanofibrous mats, respectively.

5.3. Limitations of surface analytical methods and optical determination of lignin immobilization

The XPS results for larger particles are in good agreement with the visual assessment by SEM. Both methods confirmed the successful immobilization of 300NPs and MPs without apparent differences among NF modifications. In the case of small particles, only the XPS results for amine-coated NFs corresponded clearly to SEM, proving the binding of 15NPs and 50NPs. Nevertheless, the chemical compositions of pristine and O_2-treated NFs with small particles, even though burdened with uncertainty, also supported findings drawn from SEM:

- 15NPs on pristine NFs were clearly present on SEM micrographs (Fig. 7), in agreement with the increase of oxygen compared to rinsed reference (Fig. 8a).
- 50NPs on pristine NFs and both types of small particles on O_2-treated NFs were not confirmed by either method.

The XPS results for carboxyl-PP-coated NFs with both types of small particles differ from the SEM results. Whereas f indicated a lignin coverage of at least 20% (similar to amine-PP-coated NFs, Fig. 8b), visual inspection by SEM (Fig. S15 and S16) showed only a limited number of 15NPs and 50NPs on carboxyl PPs.

The discrepancies between conclusions drawn from XPS and SEM showed that they alone are not a conclusive tool for evaluating lignin immobilization. Moreover, both methods analyze only the surface of the nanofibrous substrate. To also take into account the information from the bulk of NF mats, we determined the amount of all immobilized lignin indirectly from the difference in the lignin mass in the colloid/suspension before and after immobilization using UV–Vis spectroscopy. The results are shown as relative values in Fig. 9a (before washing) and as absolute values in μ g in Fig. S20a (before washing).

Based on UV–Vis spectroscopy, we can confirm that all NF mats were capable of immobilizing at least some portion of lignin particles. However, at most ~15% of lignin was immobilized from the initial mass in colloid/suspension. This binding capacity was reached for all types of particles on amine-PP-coated NFs. Although carboxyl PP coatings were not so effective for 50NPs, the results for other particles are comparable to amine PPs. Interestingly, pristine NFs were also able to collect at least 10% of particles from initial colloid/suspensions; they were as good as amine PPs for 15NPs and 300NPs. O_2 treatment was the least efficient of the studied surface modifications, with the lowest amount of attached lignin particles.

Comparing Figs. 7–9, we can conclude that even though MPs were present on the surface of all tested NFs (shown by SEM and XPS), the NFs coated with PPs contained more MPs inside nanofibrous mats (deduced from UV–Vis). The 300NPs were distributed on the surface of all NF mats (shown by SEM and XPS). However, O_2-treated NFs contained half the amount of 300NPs compared to other modifications (shown by UV–Vis), indicating that 300NPs were mainly on the surface and did not enter the NF bulk much. On the other hand, small particles (15NPs and 50NPs) were not confirmed in high numbers on the surface of pristine and carboxyl-PP-coated NF mats (with the exception of 15NPs on pristine NFs). Still, a decrease in their amounts in immobilization colloids suggests their presence inside nanofibrous mats. For O_2-treatment, small particles were not present in a substantial amount either on the mat surface or in the bulk. A schematic representation of where, if on the nanofibrous mat surface and/or in the bulk, and in what numbers lignin particles were most likely located using different surface modifications is given in Fig. 10.

5.4. Stability of lignin particle binding to PCL nanofibrous mats

Lignin nano/microparticles were at least partially bound to all, *i. e.,* pristine, O_2-treated, carboxyl-PP-coated, and amine-PP-coated NFs. The question remains, how firmly they are attached. Whether they stay when immersed in an aqueous environment again or are released into the liquid. To evaluate the binding stability, NF mats with immobilized lignin were washed in water, and both the water and the mats were analyzed afterwards. Comparing SEM micrographs of NFs before and after washing (see Fig. S21–24), no clear differences can be distinguished. If lignin was recognizable after immobilization, it was still there after washing.

By UV–Vis spectroscopy, we detected only a small number of lignin particles in washing water. Since this method analyses the total amount of lignin released either from the NF mat surface or from its porous bulk, we concluded that more than 80% of the immobilized particles are trapped firmly in porous NF mats (Fig. 9b).

The total release of immobilized MPs from any NF mats tends to be higher than the rest of the particles (Fig. 9b). Since they are much larger than other studied particles, they are in contact with NFs only through a limited area with respect to particle size. Therefore, the binding to

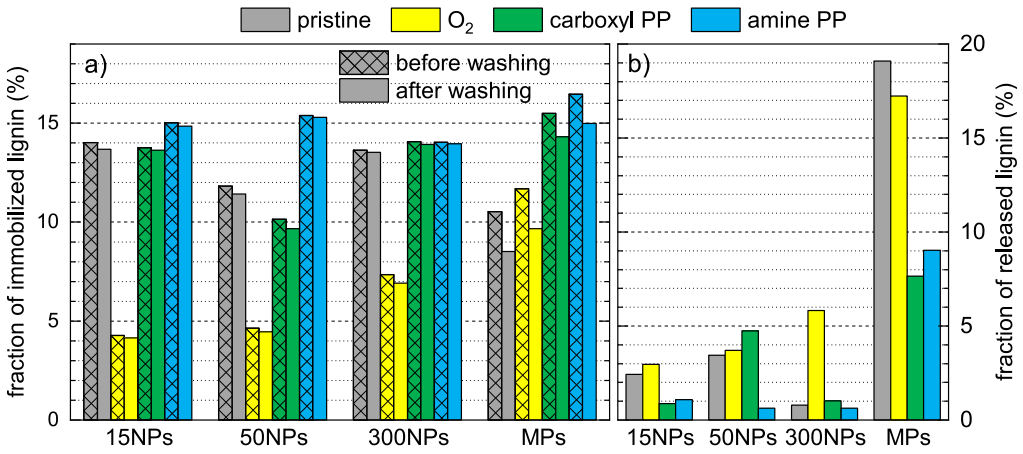

Fig. 9. (a) Fraction of lignin immobilized from the initial solution/suspension on pristine and plasma-modified PCL nanofibrous mats: before washing — lignin fraction directly after immobilization, after washing — lignin fraction left after subsequent washing. (b) Fraction of immobilized lignin released from pristine and plasma-modified PCL nanofibrous mats after washing. The results were determined based on UV–Vis spectroscopy. The initial concentrations of immobilization solution/suspension are given in part Section 2.4; MPs were used at concentrations of 3.8 mg/ml.

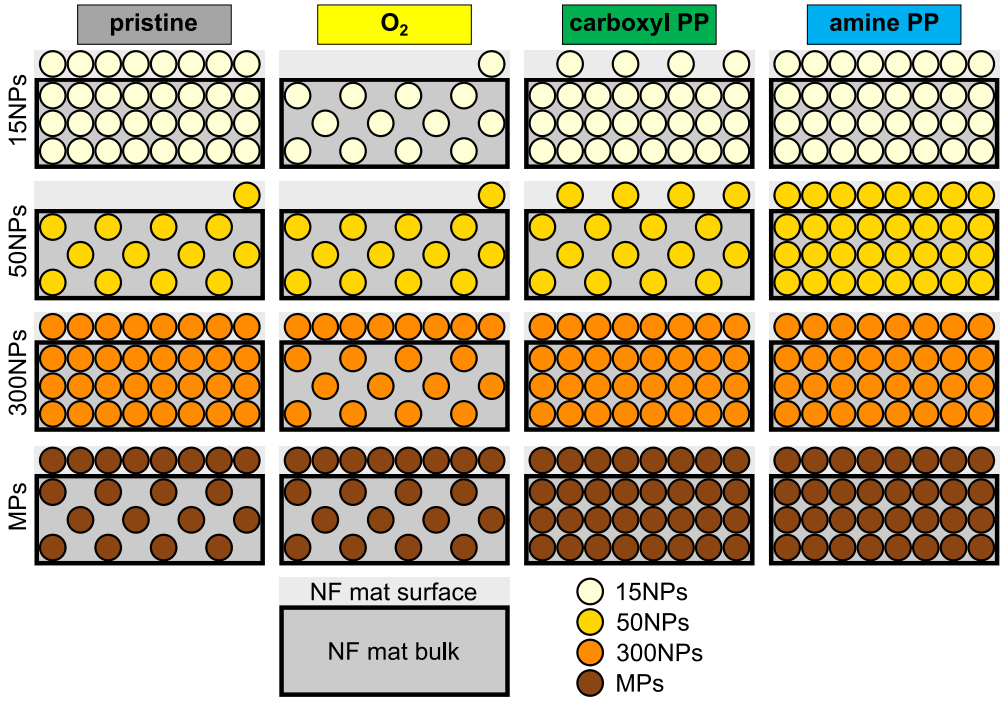

Fig. 10. Schematic representation of lignin particle presence on pristine and plasma-modified nanofibrous mat surface and/or in its bulk after immobilization.

NFs is not so firm, and they disengage more easily from the surface. Moreover, the absolute amount of released MPs was similar for all NF mats (Fig. S20b), suggesting that some MPs stick only mechanically and are released regardless of the surface modification.

A change of the surface composition before and after washing the NF mats with immobilized lignin (Fig. 8a) suggested a partial removal of all types of NPs from the surface of pristine NFs. However, the total release of NPs from pristine NFs was below 4% of the immobilized amount (Fig. 9b).

Although a negligible change of the surface composition before and after washing for O_2-treated NFs with 15NPs and 50NPs proposes their stability on the surface, we have to consider that the amount of immobilized particles was the lowest (below 5%, see Fig. 9a). When a slightly higher amount of 300NPs was immobilized on O_2-treated NFs, a significant release was observed for both the surface characterization with XPS and the total release determined with UV–Vis measurements.

The NF mats coated with carboxyl or amine PPs exhibited a good efficiency (14%) for the total immobilized amount of 300 NPs and high surface coverage (0.8 and 0.45, respectively). However, the surface coverage after washing decreased to the values typical for smaller NPs on PPs (about 0.3), despite quite low total release (below 2%).

In the case of NFs coated with carboxyl PP, 50NPs exhibited quite low total immobilization and the lowest surface coverage from all the particles on PP coatings. Moreover, these bad results were combined with non-negligible total release and high surface release (nothing left on the surface). On the contrary, 15NPs proved good total and surface immobilization, low total release, but surprisingly high surface release (almost nothing left). In conclusion, the surface attachment was not permanent for 15NPs and 50NPs on carboxyl PPs.

Contrary to carboxyl PP surfaces, 15NPs and 50NPs immobilized through amine PPs stuck to the surface very well, and the total release from the whole NF mats was only 1% at maximum, *i. e.*, either markedly

lower than on other types of NFs (for 50NPs) or comparably low as on carboxyl PPs (for 15NPs, 300NPs and MPs) or pristine NFs (for 300NPs). A schematic representation of lignin particle release from pristine and plasma-modified nanofibrous mats after washing can be found in Fig. S25.

5.5. Mechanisms of lignin particle immobilization

We demonstrated that NF coating by amine PP thin film was the most effective and, at the same time, the most universal surface modification to permanently immobilize all studied types of lignin particles. The immobilization utilized the positive surface charge that amino groups in amine PP coating acquire through protonation after immersion in an aqueous environment [55]. Since all lignin particles exhibit negative surface charge (Table 1), electrostatic interactions between positive and negative counterparts resulted in lignin particle binding. Moreover, the penetration depth of amine PP deposition inside the nanofibrous mat is up to 70 μm [41]. Thanks to that, lignin particles were immobilized on the surface as well as inside nanofibrous mats. The interaction was strong enough to preserve lignin particle attachment after repeated exposure to water. Therefore, coating with amine PPs proved advantageous for firmly binding the negatively charged particles.

In contrast, O_2-plasma treatment was the worst among the evaluated modifications for lignin immobilization. Although the lignin colloid/suspension penetrated the nanofibrous structure easily due to its increased wettability after O_2-plasma treatment, the negative surface charge of oxygen-containing groups repulsed negatively charged lignin particles and prevented them from binding. Thus, a small amount of lignin can be carried by nanofibrous mats treated by O_2-plasma thanks to the mechanical interlocking of nano/microparticles and nanostructured and porous mats, but it is easily released when immersed in water.

The carboxyl-PP-coated and pristine NFs exhibited similar water contact angle, 119–121°. Thus, the question is how lignin particles can bind to such hydrophobic (non-polar) surfaces. However, except for polar (hydrophilic) domains created by hydroxyl and carboxylic groups, lignin contains, to a lesser extent, aromatic rings and hydrocarbon chains contributing to its partly nonpolar (hydrophobic) character [75]. Therefore, lignin can exhibit amphiphilic behavior and immobilize at hydrophobic surfaces by hydrophobic interactions.

6. Conclusion

Four types of lignin particles in a wide range of sizes (average diameter of 15, 50, 300 nm and 2 μm) were synthesized from kraft lignin. We verified the size-dependent effect of lignin particles in suspension on both gram-negative bacteria (*E. coli*) and cells (fibroblasts and keratinocytes) *in vitro*. While small particles (15 and 50 nm) did not have an antimicrobial effect and the cell viability was only partially reduced at high concentrations, 300 nm particles in the concentration of 0.4 mg/ml reduced bacteria growth by the ALR >7.4, but simultaneously, killed all tested cells. Antibacterial effect diminished for further increased particle size, *i. e.* microparticles. Therefore, balancing antimicrobial activity with cytocompatibility of lignin particles proved challenging, emphasizing the necessity of concurrently evaluating both properties in bioapplications.

For immobilization of lignin particles on a supporting matrix, we explored electrospun polymer nanofibrous mats and their various surface modifications using plasma processing (O_2-plasma treatment and coating with carboxyl or amine plasma polymer thin films). Dip-coating of lignin particles from a water colloid/suspension on the NF mats was established as the most reproducible and homogeneous immobilization method. To answer conclusively whether and to what extent lignin particles were attached to NFs, two surface methods (SEM, XPS) and one optical analytical method (UV–Vis) had to be combined. Overall, up to ~15% of lignin initial mass from colloid/suspension was bound to NF mats, resulting in a high coverage of NF surface (up to 50%).

We proved that amine PP coating of NFs is the most versatile and effective way to firmly immobilize lignin nano/microparticles with stable binding in an aqueous environment. The attachment can be explained through the electrostatic interactions between positively charged amino groups in PPs and negatively charged phenol groups of lignin. O_2-plasma treatment was ineffective, which can be associated with repulsion between oxygen-containing polar groups created on the surface and lignin particles, both negatively charged. Although carboxyl PPs performed satisfactorily, they brought no benefit over amine PPs. Surprisingly, pristine NFs without any modification were also able to bind a noticeable amount of lignin particles. Since the water contact angle of pristine and carboxyl-PP-coated NFs was similar, 119–121°, we proposed that these mats immobilize lignin particles through hydrophobic interactions.

CRediT authorship contribution statement

Lucie Janů: Writing – review & editing, Writing – original draft, Visualization, Validation, Project administration, Methodology, Investigation, Formal analysis. **Nada Souawda:** Writing – original draft, Resources, Investigation. **Resmi Anand:** Validation, Resources, Methodology. **David Duday:** Supervision, Funding acquisition, Conceptualization. **Jiřina Medalová:** Methodology, Investigation. **Delphine Collard:** Methodology, Investigation, Formal analysis. **David Nečas:** Writing – review & editing, Visualization, Methodology, Formal analysis. **Kateřina Polášková:** Investigation. **Petr Ryšánek:** Resources. **Jean-Sébastien Thomann:** Conceptualization. **Martina Janůšová:** Investigation. **Lenka Zajíčková:** Writing – review & editing, Validation, Supervision, Project administration, Funding acquisition, Conceptualization.

Declaration of competing interest

The authors declare no conflict of interest.

Acknowledgments

This research was carried out under the project 24-12321S supported by the Czech Science Foundation and the M-Era.net LIGNP4WOUND project (Project number: 7371), partially supported by the Technology Agency of the Czech Republic (TH71020007). CzechNanoLab project LM2023051 funded by MEYS CR is gratefully acknowledged for the financial support of the sample fabrication and measurements at CEITEC Nano Research Infrastructure. The authors also acknowledge the assistance provided by the Research Infrastructure NanoEnviCz with the project number LM2023066.

Appendix A. Supplementary data

Supplementary material related to this article can be found online at https://doi.org/10.1016/j.ijbiomac.2026.150226.

Data availability

Data will be made available on request.

References

[1] J. Gil-Chávez, P. Gurikov, X. Hu, R. Meyer, W. Reynolds, I. Smirnova, Application of novel and technical lignins in food and pharmaceutical industries: Structure-function relationship and current challenges, Biomass Convers. Biorefin. 11 (2021) 2387–2403, http://dx.doi.org/10.1007/s13399-019-00458-6.

[2] M.K. Haider, D. Kharaghani, L. Sun, S. Ullah, M.N. Sarwar, A. Ullah, M. Khatri, Y. Yoshiko, M. Gopiraman, I.S. Kim, Synthesized bioactive lignin nanoparticles/polycaprolactone nanofibers: A novel nanobiocomposite for bone tissue engineering, Biomater. Adv. 144 (2023) 213203, http://dx.doi.org/10.1016/j.bioadv.2022.213203.

[3] W. Yang, E. Fortunati, D. Gao, G.M. Balestra, G. Giovanale, X. He, L. Torre, J.M. Kenny, D. Puglia, Valorization of acid isolated high yield lignin nanoparticles as innovative antioxidant/antimicrobial organic materials, ACS Sustain. Chem. Eng. 6 (3) (2018) 3502–3514, http://dx.doi.org/10.1021/acssuschemeng.7b03782.

[4] A.G. Morena, T. Tzanov, Antibacterial lignin-based nanoparticles and their use in composite materials, Nanoscale Adv. 4 (21) (2022) 4447–4469, http://dx.doi.org/10.1039/d2na00423b.

[5] C. Vasile, M. Baican, Lignins as promising renewable biopolymers and bioactive compounds for high-performance materials, Polymers 15 (15) (2023) 3177, http://dx.doi.org/10.3390/polym15153177.

[6] S. Sugiarto, Y. Leow, C.L. Tan, G. Wang, D. Kai, How far is Lignin from being a biomedical material? Bioact. Mater. 8 (2022) 71–94, http://dx.doi.org/10.1016/j.bioactmat.2021.06.023.

[7] A. Henn, M.-L. Mattinen, Chemo-enzymatically prepared lignin nanoparticles for value-added applications, World J. Microbiol. Biotechnol. 35 (2019) 1–9, http://dx.doi.org/10.1007/s11274-019-2697-7.

[8] M. Österberg, M.H. Sipponen, B.D. Mattos, O.J. Rojas, Spherical lignin particles: a review on their sustainability and applications, Green Chem. 22 (9) (2020) 2712–2733, http://dx.doi.org/10.1039/d0gc00096e.

[9] W.D.H. Schneider, A.J.P. Dillon, M. Camassola, Lignin nanoparticles enter the scene: A promising versatile green tool for multiple applications, Biotechnol. Adv. 47 (2021) 107685, http://dx.doi.org/10.1016/j.biotechadv.2020.107685.

[10] J. Bang, S. Jung, H. Yun, H.-J. Jin, H.-W. Kwak, Effect of Lignin nanoparticle addition on the physicochemical properties of electrospun poly(vinyl alcohol) nanofibers, Polym. Korea 47 (2023) 720–728, http://dx.doi.org/10.7317/pk.2023.47.6.720.

[11] S. Amini, A. Saudi, N. Amirpour, M. Jahromi, S.S. Najafabadi, M. Kazemi, M. Rafienia, H. Salehi, Application of electrospun polycaprolactone fibers embedding lignin nanoparticle for peripheral nerve regeneration: in vitro and in vivo study, Int. J. Biol. Macromol. 159 (2020) 154–173, http://dx.doi.org/10.1016/j.ijbiomac.2020.05.073.

[12] J. Geltmeyer, H. Teixido, M. Meire, T.V. Acker, K. Deventer, F. Vanhaecke, S.V. Hulle, K.D. Buysser, K.D. Clerck, TiO2 functionalized nanofibrous membranes for removal of organic (micro)pollutants from water, Sep. Purif. Technol. 179 (2017) 533–541, http://dx.doi.org/10.1016/j.seppur.2017.02.037.

[13] H. Wang, X. Huang, W. Li, J. Gao, H. Xue, R.K. Li, Y.W. Mai, TiO2 nanoparticle decorated carbon nanofibers for removal of organic dyes, Colloid. Surf. A 549 (2018) 205–211, http://dx.doi.org/10.1016/j.colsurfa.2018.04.017.

[14] E. Jeoung, Y.C. Yeh, T. Nelson, T. Kushida, L.S. Wang, R. Mout, X. Li, K. Saha, A. Gupta, G.Y. Tonga, J.J. Lannutti, V.M. Rotello, Fabrication of functional nanofibers through post-nanoparticle functionalization, Macromol. Rapid Commun. 36 (2015) 678–683, http://dx.doi.org/10.1002/marc.201400744.

[15] E. Sapountzi, M. Braiek, F. Vocanson, J.F. Chateaux, N. Jaffrezic-Renault, F. Lagarde, Gold nanoparticles assembly on electrospun poly(vinyl alcohol)/poly(ethyleneimine)/glucose oxidase nanofibers for ultrasensitive electrochemical glucose biosensing, Sensors Actuators B 238 (2017) 392–401, http://dx.doi.org/10.1016/j.snb.2016.07.062.

[16] R.S. Gill, R.F. Saraf, S. Kundu, Self-assembly of gold nanoparticles on poly(allylamine hydrochloride) nanofiber: A new route to fabricate "necklace" as single electron devices, ACS Appl. Mater. Interfaces 5 (2013) 9949–9956, http://dx.doi.org/10.1021/am401864j.

[17] Y. man Liu, Q. Li, H. huan Liu, H. hui Cheng, J. Yu, Z. xia Guo, Antibacterial thermoplastic polyurethane electrospun fiber mats prepared by 3-aminopropyltriethoxysilane-assisted adsorption of Ag nanoparticles, Chin. J. Polym. Sci. (Engl. Ed.) 35 (2017) 713–720, http://dx.doi.org/10.1007/s10118-017-1928-3.

[18] R.S. Andre, A. Pavinatto, L.A. Mercante, E.C. Paris, L.H. Mattoso, D.S. Correa, Improving the electrochemical properties of polyamide 6/polyaniline electrospun nanofibers by surface modification with ZnO nanoparticles, RSC Adv. 5 (2015) 73875–73881, http://dx.doi.org/10.1039/c5ra15588f.

[19] P. Li, M. Zhang, X. Liu, Z. Su, G. Wei, Electrostatic assembly of platinum nanoparticles along electrospun polymeric nanofibers for high performance electrochemical sensors, Nanomaterials 7 (2017) http://dx.doi.org/10.3390/nano7090236.

[20] Y. Liu, P. Cheng, Q. Guo, N. Liu, Y. Wan, W. Zhong, Z. Lu, K. Liu, G. Sun, D. Wang, Ag nanoparticles decorated PVA-co-PE nanofibrous microfiltration membrane with antifouling surface for efficient sterilization, Compos. Commun. 21 (2020) http://dx.doi.org/10.1016/j.coco.2020.100379.

[21] H.H. Cheng, F. Chen, J. Yu, Z.X. Guo, Gold-nanoparticle-decorated thermoplastic polyurethane electrospun fibers prepared through a chitosan linkage for catalytic applications, J. Appl. Polym. Sci. 134 (2017) http://dx.doi.org/10.1002/app.44336.

[22] R. Yaseri, M. Fadaie, E. Mirzaei, H. Samadian, A. Ebrahiminezhad, Surface modification of polycaprolactone nanofibers through hydrolysis and aminolysis: a comparative study on structural characteristics, mechanical properties, and cellular performance, Sci. Rep. 13 (1) (2023) 9434, http://dx.doi.org/10.1038/s41598-023-36563-w.

[23] B.S. Tucker, S. Aliakbarshirazi, V.M. Vijayan, M. Thukkaram, N. De Geyter, V. Thomas, Nonthermal plasma processing for nanostructured biomaterials and tissue engineering scaffolds: A mini review, Curr. Opin. Biomed. Eng. 17 (2021) 100259, http://dx.doi.org/10.1016/j.cobme.2020.100259.

[24] K. Vasilev, A. Casanal, H. Challougui, H.J. Griesser, Template-assisted generation of nanocavities within plasma polymer films, J. Phys. Chem. B 113 (2009) 7059–7063, http://dx.doi.org/10.1021/jp807986k.

[25] K. Vasilev, V.R. Sah, R.V. Goreham, C. Ndi, R.D. Short, H.J. Griesser, Antibacterial surfaces by adsorptive binding of polyvinyl-sulphonate- stabilized silver nanoparticles, Nanotechnology 21 (2010) http://dx.doi.org/10.1088/0957-4484/21/21/215102.

[26] R.V. Goreham, A. Mierczynska, M. Pierce, R.D. Short, S. Taheri, A. Bachhuka, A. Cavallaro, L.E. Smith, K. Vasilev, A substrate independent approach for generation of surface gradients, Thin Solid Films 528 (2013) 106–110, http://dx.doi.org/10.1016/j.tsf.2012.04.087.

[27] R.V. Goreham, R.D. Short, K. Vasilev, Method for the generation of surface-bound nanoparticle density gradients, J. Phys. Chem. C 115 (2011) 3429–3433, http://dx.doi.org/10.1021/jp111221g.

[28] X. Liu, Y. Wang, Y. He, X. Wang, R. Zhang, A. Bachhuka, R.M. Visalakshan, Q. Feng, K. Vasilev, Synergistic effect of surface chemistry and surface topography gradient on osteogenic/adipogenic differentiation of hMSCs, ACS Appl. Mater. Interfaces 13 (2021) 30306–30316, http://dx.doi.org/10.1021/acsami.1c03915.

[29] R. Sekine, M. Khaksar, G. Brunetti, E. Donner, K.G. Scheckel, E. Lombi, K. Vasilev, Surface immobilization of engineered nanomaterials for in situ study of their environmental transformations and fate, Environ. Sci. Technol. 47 (2013) 9308–9316, http://dx.doi.org/10.1021/es400839h.

[30] R.M. Visalakshan, M.N. Macgregor, A.A. Cavallaro, S. Sasidharan, A. Bachhuka, A.M. Mierczynska-Vasilev, J.D. Hayball, K. Vasilev, Creating nano-engineered biomaterials with well-defined surface descriptors, ACS Appl. Nano Mater. 1 (2018) 2796–2807, http://dx.doi.org/10.1021/acsanm.8b00458.

[31] R.M. Visalakshan, A.A. Cavallaro, M.N. MacGregor, E.P. Lawrence, K. Koynov, J.D. Hayball, K. Vasilev, Nanotopography-induced unfolding of fibrinogen modulates leukocyte binding and activation, Adv. Funct. Mater. 29 (2019) http://dx.doi.org/10.1002/adfm.201807453.

[32] P.R.L. Dabare, A. Bachhuka, J.Y. Quek, L.F. Marsal, J. Hayball, K. Vasilev, Nano-roughness-mediated macrophage polarization for desired host immune response, Small Sci. 3 (2023) http://dx.doi.org/10.1002/smsc.202300080.

[33] N. Ninan, B. Pidhatika, R. Bright, B.M. Kartika, R.P. Rudianto, Y.A. Swasono, R. Ardhani, K. Vasilev, Advancing sustainable technologies: plasma-engineered bioplastics with silver nanoparticle integration, J. Mater. Sci. 59 (2024) 9003–9020, http://dx.doi.org/10.1007/s10853-024-09673-7.

[34] H. Wang, C. Wang, C. Lei, Z. Wu, G. Shen, R. Yu, A novel biosensing interfacial design produced by assembling nano-Au particles on amine-terminated plasma-polymerized films, Anal. Bioanal. Chem. 377 (2003) 632–638, http://dx.doi.org/10.1007/s00216-003-2166-9.

[35] H. Zeng, H. Wang, F. Chen, H. Xin, G. Wang, L. Xiao, K. Song, D. Wu, Q. He, G. Shen, Development of quartz-crystal-microbalance-based immunosensor array for clinical immunophenotyping of acute leukemias, Anal. Biochem. 351 (2006) 69–76, http://dx.doi.org/10.1016/j.ab.2005.12.006.

[36] X. Rao, A.A. Hassan, C. Guyon, M. Zhang, S. Ognier, M. Tatoulian, Plasma polymer layers with primary amino groups for immobilization of nano- and microparticles, Plasma Chem. Plasma Process. 40 (2020) 589–606, http://dx.doi.org/10.1007/s11090-019-10056-z.

[37] S. Taheri, G. Baier, P. Majewski, M. Barton, R. Förch, K. Landfester, K. Vasilev, Synthesis and surface immobilization of antibacterial hybrid silver-poly(l-lactide) nanoparticles, Nanotechnology 25 (2014) http://dx.doi.org/10.1088/0957-4484/25/30/305102.

[38] S. Taheri, A. Cavallaro, S.N. Christo, P. Majewski, M. Barton, J.D. Hayball, K. Vasilev, Antibacterial plasma polymer films conjugated with phospholipid encapsulated silver nanoparticles, ACS Biomater. Sci. Eng. 1 (2015) 1278–1286, http://dx.doi.org/10.1021/acsbiomaterials.5b00338.

[39] B. Joseph, N. Ninan, R.M. Visalakshan, C. Denoual, R. Bright, N. Kalarikkal, Y. Grohens, K. Vasilev, S. Thomas, Insights into the biomechanical properties of plasma treated 3D printed PCL scaffolds decorated with gold nanoparticles, Compos. Sci. Technol. 202 (2021) http://dx.doi.org/10.1016/j.compscitech.2020.108544.

[40] A. Aksit, N.O. Camlibel, E.T. Zeren, B. Kutlu, Development of antibacterial fabrics by treatment with Ag-doped TiO2 nanoparticles, J. Text. Inst. 108 (2017) 2046–2056, http://dx.doi.org/10.1080/00405000.2017.1311766.

[41] M. Michlíček, L. Blahová, E. Dvořáková, D. Nečas, L. Zajíčková, Deposition penetration depth and sticking probability in plasma polymerization of cyclopropylamine, Appl. Surf. Sci. 540 (2021) http://dx.doi.org/10.1016/j.apsusc.2020.147979.
[42] M. Abrigo, P. Kingshott, S.L. McArthur, Bacterial response to different surface chemistries fabricated by plasma polymerization on electrospun nanofibers, Biointerphases 10 (4) (2015) http://dx.doi.org/10.1116/1.4927218.
[43] Y. Cruz, E. Muñoz, E.Y. Gomez-Pachón, J. Morales-Corona, J. Olayo-Lortia, R. Olayo, R. Olayo-Valles, Electrospun PCL-protein scaffolds coated by pyrrole plasma polymerization, J. Biomater. Sci. Polym. Ed. 30 (2019) 832–845, http://dx.doi.org/10.1080/09205063.2019.1603338.
[44] D.M. Osorio-Londoño, J.R. Godínez-Fernández, M.C. Acosta-García, J. Morales-Corona, R. Olayo-González, A. Morales-Guadarrama, Pyrrole plasma polymer-coated electrospun scaffolds for neural tissue engineering, Polymers 13 (2021) http://dx.doi.org/10.3390/polym13223876.
[45] A. Manakhov, D. Nečas, J. Čechal, D. Pavliňák, M. Eliáš, L. Zajíčková, Deposition of stable amine coating onto polycaprolactone nanofibers by low pressure cyclopropylamine plasma polymerization, Thin Solid Films 581 (2015) 7–13, http://dx.doi.org/10.1016/j.tsf.2014.09.015.
[46] S. Miroshnichenko, V. Timofeeva, E. Permyakova, S. Ershov, P. Kiryukhantsev-Korneev, E. Dvořaková, D.V. Shtansky, L. Zajíčková, A. Solovieva, A. Manakhov, Plasma-coated polycaprolactone nanofibers with covalently bonded platelet-rich plasma enhance adhesion and growth of human fibroblasts, Nanomaterials 9 (2019) 637, http://dx.doi.org/10.3390/nano9040637.
[47] A. Manakhov, E. Kedroňová, J. Medalová, P. Černochová, A. Obrusník, M. Michlíček, D.V. Shtansky, L. Zajíčková, Carboxyl-anhydride and amine plasma coating of PCL nanofibers to improve their bioactivity, Mater. Des. 132 (2017) 257–265, http://dx.doi.org/10.1016/j.matdes.2017.06.057.
[48] I. Nemcakova, L. Blahova, P. Rysanek, A. Blanquer, L. Bacakova, L. Zajíčková, Behaviour of vascular smooth muscle cells on amine plasma-coated materials with various chemical structures and morphologies, Int. J. Mol. Sci. 21 (2020) 1–24, http://dx.doi.org/10.3390/ijms21249467.
[49] A. Manisekaran, P. Grysan, B. Duez, D.F. Schmidt, D. Lenoble, J.-S. Thomann, Solvents drive self-assembly mechanisms and inherent properties of Kraft lignin nanoparticles (<50 nm), J. Colloid Interface Sci. 626 (2022) 178–192, http://dx.doi.org/10.1016/j.jcis.2022.06.089.
[50] A. Barry, W. Craig, H. Nadler, B. Reller, C. Sanders, J. Swenson, Methods for Determining Bactericidal Activity of Antimicrobial Agents : Approved Guideline. CLSI M26-1, NCCLS, Clinical and Laboratory Standards Institute, 940 West Valley Road Suite 2500, Wayne, Pennsylvania 19087, USA, 1999.
[51] V. Kupka, E. Dvořáková, A. Manakhov, M. Michlíček, J. Petruš, L. Vojtová, L. Zajíčková, Well-blended PCL/PEO electrospun nanofibers with functional properties enhanced by plasma processing, Polymers 12 (2020) http://dx.doi.org/10.3390/polym12061403.
[52] L. Štrbková, A. Manakhov, L. Zajíčková, A. Stoica, P. Veselý, R. Chmelík, The adhesion of normal human dermal fibroblasts to the cyclopropylamine plasma polymers studied by holographic microscopy, Surf. Coat. Technol. 295 (2016) 70–77, http://dx.doi.org/10.1016/j.surfcoat.2015.10.076.
[53] A. Manakhov, M. Landová, J. Medalová, M. Michlíček, J. Polčák, D. Nečas, L. Zajíčková, Cyclopropylamine plasma polymers for increased cell adhesion and growth, Plasma Process. Polym. 14 (7) (2017) 1600123, http://dx.doi.org/10.1002/ppap.201600123.
[54] P. Rupper, M. Vandenbossche, L. Bernard, D. Hegemann, M. Heuberger, Composition and stability of plasma polymer films exhibiting vertical chemical gradients, Langmuir 33 (2017) 2340–2352, http://dx.doi.org/10.1021/acs.langmuir.6b04600.
[55] M. Buchtelová, L. Blahová, D. Nečas, P. Křížková, J. Bartošíková, J. Medalová, Z. Kolská, D. Hegemann, L. Zajíčková, Insight into peculiar adhesion of cells to plasma-chemically prepared multifunctional "amino-glue" surfaces, Plasma Process. Polym. (2023) http://dx.doi.org/10.1002/ppap.202200157.
[56] G. Beamson, D. Briggs, High Resolution XPS Of Organic Polymers, The Scienta ESCA300 Database, John Wiley & Sons, Chichester, England, 1992, p. 295.
[57] A. Skulcova, V. Majova, M. Kohutova, M. Grosik, J. Sima, M. Jablonsky, UV/Vis spectrometry as a quantification tool for Lignin solubilized in deep eutectic solvents, BioResources 12 (2017) 6713–6722, http://dx.doi.org/10.15376/biores.12.3.6713-6722.
[58] D. Savy, M. Verrillo, S. Cangemi, V. Cozzolino, Lignin nanoparticles from hydrotropic fractionation of giant reed and eucalypt: Structural elucidation and antibacterial properties, Int. J. Biol. Macromol. 262 (2024) http://dx.doi.org/10.1016/j.ijbiomac.2024.129966.
[59] I.C. Tanganini, C.H. Camargos, J.C. Jackson, C.A. Rezende, S.R. Ceccato-Antonini, A.F. Faria, Self-assembled lignin nanoparticles produced from elephant grass leaves enable selective inactivation of Gram-positive microorganisms, RSC Sustain. 2 (2023) 459–474, http://dx.doi.org/10.1039/d3su00400g.
[60] M. Sharma, J. Marques, A. Simões, M.M. Donato, O. Cardoso, L.M. Gando-Ferreira, Optimization of lignin precipitation from black liquor using organic acids and its valorization by preparing lignin nanoparticles, Int. J. Biol. Macromol. 269 (2024) http://dx.doi.org/10.1016/j.ijbiomac.2024.131881.
[61] B.D.S. Marotti, V. Arantes, Ultra-refining for the production of long-term highly pH-stable lignin nanoparticles in high yield with high uniformity, Green Chem. 24 (2022) 1238–1258, http://dx.doi.org/10.1039/d1gc03525h.
[62] F.M. Freitas, M.A. Cerqueira, C. Gonçalves, S. Azinheiro, A. Garrido-Maestu, A.A. Vicente, L.M. Pastrana, J.A. Teixeira, M. Michelin, Green synthesis of lignin nano- and micro-particles: Physicochemical characterization, bioactive properties and cytotoxicity assessment, Int. J. Biol. Macromol. 163 (2020) 1798–1809, http://dx.doi.org/10.1016/j.ijbiomac.2020.09.110.
[63] M.A. Ali, N.M. Abdel-Moein, A.S. Owis, S.E. Ahmed, E.A. Hanafy, Preparation, characterization, antioxidant and antimicrobial activities of Lignin and eco-friendly lignin nanoparticles from Egyptian cotton stalks, Egypt. J. Chem. 65 (2022) 703–716, http://dx.doi.org/10.21608/EJCHEM.2021.86987.4221.
[64] Y. He, H. Ye, H. Li, G. Miao, Y. Hu, X. Zeng, T. You, F. Xu, Fabrication of lignin nanoparticles with adjustable size, antioxidant, antibacterial, and hydrophobic properties by a two-step fractionation, Int. J. Biol. Macromol. 297 (2025) http://dx.doi.org/10.1016/j.ijbiomac.2025.139618.
[65] G. Kim, J. Park, B.M. Kim, J. Kim, K.J. Kim, J. Park, Influence of nanoprecipitation techniques on lignin nanoparticle structure, Colloid. Surf. A 682 (2024) http://dx.doi.org/10.1016/j.colsurfa.2023.132803.
[66] R. Morcillo-Martín, M. Borrega, S. Bertella, P. Widsten, E. Rincón, E. Espinosa, A. Rodríguez, Lignin micro/nanoparticles from alternative biomass sources for neutral-pH Pickering emulsions and quercetin encapsulation, Int. J. Biol. Macromol. 310 (2025) http://dx.doi.org/10.1016/j.ijbiomac.2025.143223.
[67] H. Arakawa, M. Maeda, S. Okubo, T. Shimamura, Role of hydrogen peroxide in bactericidal action of catechin, Biol. Pharm. Bull. 27 (2004) 277–281, http://dx.doi.org/10.1248/bpb.27.277.
[68] D. Piccinino, E. Capecchi, I. Delfino, M. Crucianelli, N. Conte, D. Avitabile, R. Saladino, Green and scalable preparation of colloidal suspension of Lignin nanoparticles and its application in eco-friendly sunscreen formulations, ACS Omega 6 (2021) 21444–21456, http://dx.doi.org/10.1021/acsomega.1c02268.
[69] L. Siddiqui, J. Bag, Seetha, D. Mittal, A. Leekha, H. Mishra, M. Mishra, A.K. Verma, P.K. Mishra, A. Ekielski, Z. Iqbal, S. Talegaonkar, Assessing the potential of lignin nanoparticles as drug carrier: Synthesis, cytotoxicity and genotoxicity studies, Int. J. Biol. Macromol. 152 (2020) 786–802, http://dx.doi.org/10.1016/j.ijbiomac.2020.02.311.
[70] X. Zhang, J. Zhang, H. Yang, C. He, Y. Ke, S. Singh, G. Cheng, Determination of the structures of Lignin subunits and nanoparticles in solution by small-angle neutron scattering: Towards improving Lignin valorization, ChemSusChem 15 (2022) http://dx.doi.org/10.1002/cssc.202201230.
[71] L. Hennings, Y. Kaufmann, R. Griffin, E. Siegel, P. Novak, P. Corry, E.G. Moros, G. Shafirstein, Dead or alive Autofluorescence distinguishes heat-fixed from viable cells, Int. J. Hyperth. 25 (2009) 355–363, http://dx.doi.org/10.1080/02656730902964357.
[72] M. Yu, H. Xin, D. He, C. Zhu, Q. Li, X. Wang, J. Zhou, Electrospray lignin nanoparticles as Pickering emulsions stabilizers with antioxidant activity, UV barrier properties and biological safety, Int. J. Biol. Macromol. 238 (2023) http://dx.doi.org/10.1016/j.ijbiomac.2023.123938.
[73] L. Janů, E. Dvořáková, K. Polášková, M. Buchtelová, P. Ryšánek, Z. Chlup, T. Kruml, O. Galmiz, D. Nečas, L. Zajíčková, Enhanced adhesion of electrospun polycaprolactone nanofibers to plasma-modified polypropylene fabric, Polymers 15 (2023) http://dx.doi.org/10.3390/polym15071686.
[74] J.J. Lee, H.S. Yu, S.J. Hong, I. Jeong, J.H. Jang, H.W. Kim, Nanofibrous membrane of collagen-polycaprolactone for cell growth and tissue regeneration, J. Mater. Sci.: Mater. Med. 20 (2009) 1927–1935, http://dx.doi.org/10.1007/s10856-009-3743-z.
[75] C. Xu, F. Ferdosian, Structure and properties of Lignin, in: Conversion of Lignin Into Bio-Based Chemicals and Materials, Springer Berlin, Heidelberg, 2017, pp. 1–12, http://dx.doi.org/10.1007/978-3-662-54959-9_1, Ch. Structure and Properties of Lignin.